© 2015. Published by The Company of Biologists Ltd | Development (2015) 142, 3734-3745 doi:10.1242/dev.125328

RESEARCH ARTICLE

Disruption of the ERK/MAPK pathway in neural crest cells as a potential cause of Pierre Robin sequence

Carolina Parada[1], Dong Han[1], Alexandre Grimaldi[1], Patricia Sarrión[1], Shery S. Park[1], Richard Pelikan[1], Pedro A. Sanchez-Lara[1,2,3] and Yang Chai[1,*]

ABSTRACT

Disrupted ERK1/2 signaling is associated with several developmental syndromes in humans. To understand the function of ERK2 (MAPK1) in the postmigratory neural crest populating the craniofacial region, we studied two mouse models: *Wnt1-Cre;Erk2*$^{fl/fl}$ and *Osr2-Cre;Erk2*$^{fl/fl}$. *Wnt1-Cre;Erk2*$^{fl/fl}$ mice exhibited cleft palate, malformed tongue, micrognathia and mandibular asymmetry. Cleft palate in these mice was associated with delay/failure of palatal shelf elevation caused by tongue malposition and micrognathia. *Osr2-Cre;Erk2*$^{fl/fl}$ mice, in which the *Erk2* deletion is restricted to the palatal mesenchyme, did not display cleft palate, suggesting that palatal clefting in *Wnt1-Cre;Erk2*$^{fl/fl}$ mice is a secondary defect. Tongues in *Wnt1-Cre;Erk2*$^{fl/fl}$ mice exhibited microglossia, malposition, disruption of the muscle patterning and compromised tendon development. The tongue phenotype was extensively rescued after culture in isolation, indicating that it might also be a secondary defect. The primary malformations in *Wnt1-Cre;Erk2*$^{fl/fl}$ mice, namely micrognathia and mandibular asymmetry, are linked to an early osteogenic differentiation defect. Collectively, our study demonstrates that mutation of *Erk2* in neural crest derivatives phenocopies the human Pierre Robin sequence and highlights the interconnection of palate, tongue and mandible development. Because the ERK pathway serves as a crucial point of convergence for multiple signaling pathways, our study will facilitate a better understanding of the molecular regulatory mechanisms of craniofacial development.

KEY WORDS: ERK pathway, Cleft palate, Glossoptosis, Micrognathia, Mandibular asymmetry, Pierre Robin sequence, Neural crest cells

INTRODUCTION

The ERK transduction pathway is one of the signaling cascades that facilitates the transmission of extracellular signals to cytoplasmic and nuclear effectors (Pearson et al., 2001) via the protein kinase cascade comprising MAPKKK (RAF), MAPKK (MEK1/2) and MAPK (ERK). Activated ERK dimers regulate targets in the cytosol and nucleus, including the serum response factor (SRF) (Pearson et al., 2001; Shaw and Saxton, 2003). Newbern and colleagues generated mouse models of inactivation of *ERK2* (*MAPK1*) as well as of upstream components of the ERK cascade [*B-Raf* (*BRAF*) and *C-Raf* (*RAF1*), *MEK1* (*MAP2K1*) and *MEK2* (*MAP2K2*)] in neural crest derivatives, which resulted in analogous craniofacial malformations to those in human, including maxillary hypoplasia, cleft palate, malformed or absent tongue, and micrognathia (Newbern et al., 2008). Neural crest-specific inactivation of Srf caused fully penetrant mandibular hypoplasia, but the maxillary prominences and tongue were unaffected (Newbern et al., 2008). These findings suggest that the mechanisms controlling mandibular development are different from those of maxilla, palate and tongue. Although the ERK pathway mediates BMP, TGFβ, FGF and EGF signals, which contribute significantly to palatogenesis (Bush and Jiang, 2012), the function of this pathway in the postmigratory neural crest populating the developing palate is still unclear.

The development of the secondary palate begins with the appearance of the palatal primordia from the maxillary process; the primordia are composed of a core of neural crest-derived mesenchyme covered by ectoderm-derived epithelium (Chai and Maxson, 2006). The palatal shelves grow vertically along the two sides of the tongue. As the mandible starts growing and the tongue descends, the palatal shelves reorient to acquire a horizontal position. This movement is known as palatal shelf elevation. Once in a horizontal position, the bilateral palatal shelves grow toward each other, establish contact along the midline, and fuse (Bush and Jiang, 2012; Ferguson, 1977, 1988; Iwata et al., 2011; Yu and Ornitz, 2011). Alterations in any of these steps may lead to a cleft palate, which is one of the most common human birth defects. The elevation process is not well understood, but may involve a heterogeneous mechanism along the anteroposterior (AP) axis (Yu and Ornitz, 2011). The anterior portions of the palatal shelves seem to elevate by rotating, whereas the middle and posterior portions change their orientation via a remodeling mechanism (Bush and Jiang, 2012). Numerous theories regarding palatal shelf elevation have been proposed and can be grouped into two categories: those positing that the shelves are elevated as a consequence of the influence of extrinsic structures; and those positing that the shelves themselves play an active role in the process (Ferguson, 1977). In humans, cleft palate due to mechanical interference with palatal shelf elevation by a malpositioned tongue and small jaw is clinically classified as Pierre Robin sequence or syndrome (PRS) (Rangeeth et al., 2011). Studies of human patients have shown that mutations in *SATB2*, *SOX9*, *BMP2* and the collagens lead to PRS-like clefting (Melkoniemi et al., 2003; Tan et al., 2013). The etiology of PRS has also been associated with a range of syndromes and chromosomal anomalies plus extrinsic fetal deformational forces, but the developmental mechanisms causing this condition are unclear, in part because of the lack of an animal model (Tan et al., 2013).

In this study, we show that disruption of the ERK pathway in neural crest derivatives in a murine model causes a primary defect affecting mandibular development, which is associated with a disturbance of the osteogenic differentiation program. In these mice, micrognathia and mandibular asymmetry result in secondary tongue malformations and cleft palate. This sequence of events during

[1]Center for Craniofacial Molecular Biology, University of Southern California, Los Angeles, CA 90033, USA. [2]Department of Pathology & Pediatrics, Keck School of Medicine, University of Southern California, Los Angeles, CA 90033, USA. [3]Children's Hospital Los Angeles, Los Angeles, CA 90027, USA.

*Author for correspondence (ychai@usc.edu)

Received 11 April 2015; Accepted 2 September 2015

Development (2015) 142, 3734-3745 doi:10.1242/dev.125328

mouse development is consistent with the phenotype of human PRS. Our study highlights how defects in one craniofacial structure can adversely affect the development of others and ultimately lead to complex craniofacial malformations.

RESULTS

Domains of ERK pathway activation during craniofacial development

Activation of the ERK pathway occurs as early as E10.5 in the frontonasal region and the branchial arches (Corson et al., 2003). To investigate the roles of the ERK signaling pathway, we analyzed the localization of active, phosphorylated (P) ERK1/2 (Mapk3/1) in the palate, tongue and mandibular primordia. In the palatal shelves, P-ERK1/2 was detectable in both the epithelium and mesenchyme from E12.5 to E14.5 (Fig. 1A-C). In the developing tongue, P-ERK1/2 was detectable in the neural crest-derived mesenchyme as well as in myogenic progenitors and muscle fibers (Fig. 1D-F). By E14.5, P-ERK1/2 was restricted to the muscular component of the tongue, with only a few cells displaying positive signal in the neural crest-derived mesenchyme. In the mandible at E12.5, P-ERK1/2 was detectable in the chondrocytes of the Meckel's cartilage located peripherally and in the neighboring condensed mesenchyme (Fig. 1G). At 13.5, when osteogenic differentiation begins in the mandible, P-ERK1/2 was restricted to the osteogenic front, the undifferentiated condensed mesenchyme surrounding the differentiated area, and the peripheral chondrocytes in the Meckel's cartilage (Fig. 1H). At E14.5, P-ERK1/2 expression persisted in the undifferentiated mesenchyme, whereas expression was undetectable in differentiated cells. Moreover, the number of positive cells in the Meckel's cartilage was reduced compared with E12.5 and E13.5 (Fig. 1I). These results suggest that the ERK pathway is active in the mesenchymal progenitors that have entered the osteogenic differentiation program and becomes inactive as differentiation progresses.

Wnt1-Cre;Erk2$^{fl/fl}$ mice exhibit severe craniofacial defects

Previously, Newbern and colleagues generated *Wnt1-Cre;Erk2$^{fl/fl}$* mice and reported that they exhibited severe craniofacial malformations (Newbern et al., 2008). In order to analyze the molecular and cellular mechanisms underlying these craniofacial defects, we generated *Wnt1-Cre;Erk2$^{fl/fl}$* mice using a pure C57BL/6 background. The craniofacial phenotype in our mice was less severe than that reported previously (Newbern et al., 2008). Our *Wnt1-Cre;Erk2$^{fl/fl}$* mice died at birth and exhibited multiple craniofacial malformations including maxillary hypoplasia, complete cleft palate, tongue defects, micrognathia, and non-preferential mandibular asymmetry (Fig. 2).

Palatal shelf elevation was compromised in *Wnt1-Cre;Erk2$^{fl/fl}$* mice. Because elevation may occur via different mechanisms in the anterior versus posterior regions of the palate (reviewed by Bush and Jiang, 2012), we analyzed microCT scan sections along the AP axis at the newborn stage, but found that all regions were affected similarly (n=3; Fig. S1A-J). The elevation defect was also detectable along the AP axis at E14.5 and E15.5 (data not shown). We also found that *Erk2* mutant mice displayed microglossia, a tongue defect not previously described (Fig. 2G-N). 3D reconstruction of microCT scans showed a ∼45% reduction in the tongue volume of *Wnt1-Cre;Erk2$^{fl/fl}$* mice (Fig. 2M-Q). In addition, *Wnt1-Cre;Erk2$^{fl/fl}$* tongues exhibited malposition and disruption of muscle patterning. Although no significant difference was detectable in HE-stained sagittal sections, malpositioning of the tongue in *Wnt1-Cre;Erk2$^{fl/fl}$* mice was evident after myosin heavy chain immunostaining of coronal sections (Fig. 2K,L). The organization of the fibers in both the intrinsic and extrinsic muscles of the tongue was altered in *Wnt1-Cre;Erk2$^{fl/fl}$* mice, resulting in a gross disruption of the muscle pattern and position. Typically, one half of the tongue was able to descend whereas the other side remained high, blocking the elevation of one palatal shelf (Fig. 2K,L). This finding was confirmed by microCT scan reconstructions (Fig. 2M,N) and is

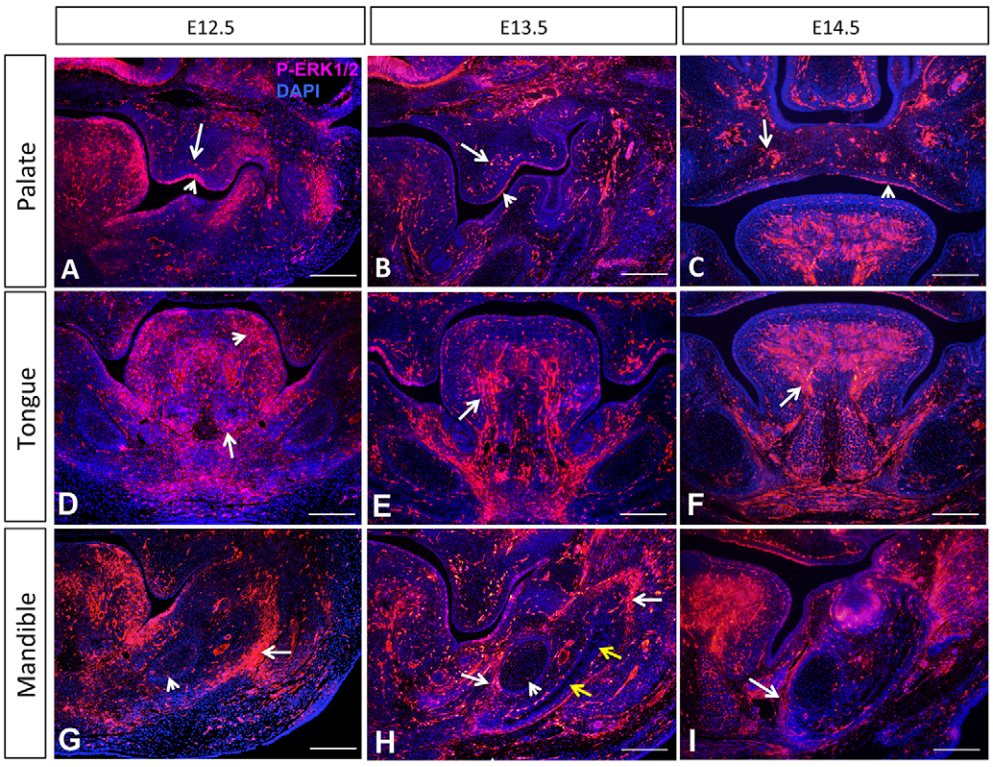

Fig. 1. Specific domains of ERK pathway activation in the craniofacial region. P-ERK1/2 immunostaining (red) in the palatal shelves (A-C), tongue primordium (D-F) and mandible (G-I) of control mice at E12.5, E13.5 and E14.5. In A-C, arrowheads indicate signals in the epithelium whereas arrows indicate signals in the mesenchyme. In D-F, arrowhead indicates signals in the neural crest-derived mesenchyme whereas arrows indicate signals in the muscle. In G-I, arrowheads indicate signals in the chondroblasts of the Meckel's cartilage whereas arrows indicate signals in the osteogenic progenitors. Yellow arrows indicate the location of terminally differentiated osteoblasts. n=3 for each stage. Scale bars: 100 µm.

Development (2015) 142, 3734-3745 doi:10.1242/dev.125328

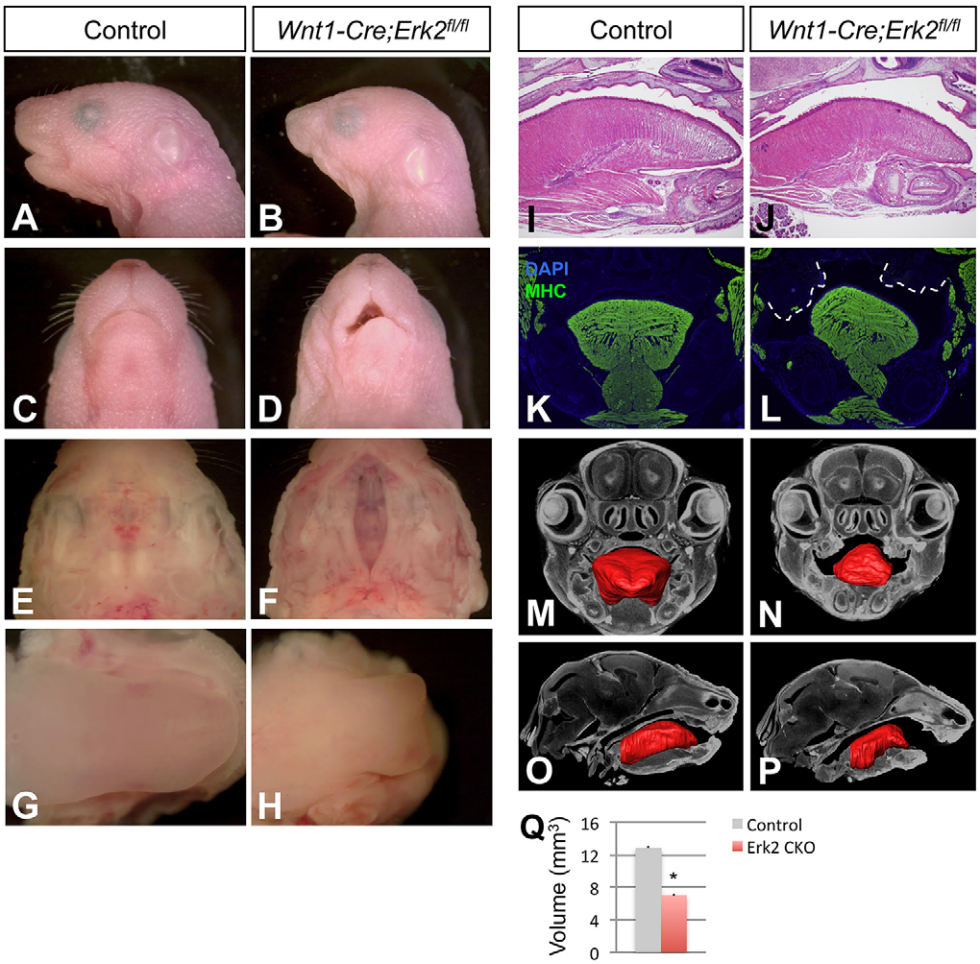

Fig. 2. *Wnt1-Cre;Erk2*$^{fl/fl}$ mice exhibit severe craniofacial malformations. (A-D) Sagittal (A,B) and ventral (C,D) views of newborn control and *Wnt1-Cre;Erk2*$^{fl/fl}$ heads. (E-H) Intraoral views of the palates (E,F) and tongues (G,H) of control and *Wnt1-Cre;Erk2*$^{fl/fl}$ newborns. (I,J) HE staining of sagittal sections of control and *Wnt1-Cre;Erk2*$^{fl/fl}$ newborn tongues. (K,L) Myosin heavy chain (MHC; green) immunostaining of coronal sections of control and *Wnt1-Cre;Erk2*$^{fl/fl}$ newborn heads. Dashed lines delineate the malformed and unfused palatal shelves in *Wnt1-Cre;Erk2*$^{fl/fl}$ mice. (M-Q) 3D reconstructions of control and *Wnt1-Cre;Erk2*$^{fl/fl}$ tongues from microCT scans. Tongue volumes of control and *Wnt1-Cre;Erk2*$^{fl/fl}$ (Erk2 CKO) samples are quantified in Q. **P*<0.05. *n*=3.

consistent with the mandibular phenotype. The mandibles of *Wnt1-Cre;Erk2*$^{fl/fl}$ mice also exhibited a severe disruption in bone development. As reported previously, *Erk2* mutant mandibles were significantly smaller than those of controls. Additionally, we observed a dramatic asymmetry in most of the mandibles (Table S1), which was associated with the asymmetry of the tongue and the elevation of a single palatal shelf. At the newborn stage, the more severely affected side of the mandible corresponded to the side lacking palatal shelf elevation (*n*=3; Fig. S1). In *Wnt1-Cre;Erk2*$^{fl/fl}$ newborns in which the micrognathia affected both sides equally, the tongue was symmetric and positioned in a high location and neither palatal shelf elevated (*n*=2; data not shown).

Cleft palate in *Wnt1-Cre;Erk2*$^{fl/fl}$ mice is a consequence of tongue malposition and micrognathia

Because the ERK transduction pathway controls diverse cellular activities, including cell migration, survival and proliferation (Pearson et al., 2001), we investigated whether any of these processes was altered in *Wnt1-Cre;Erk2*$^{fl/fl}$ palatal shelves. To analyze neural crest cell migration, we performed *lacZ* staining of whole-mount *Wnt1-Cre;R26R* (control) and *Wnt1-Cre;Erk2*$^{fl/fl}$*;R26R* embryos and frozen sections. We detected no difference at E10.5 or E11.5 (Fig. 3A,B, Fig. S2A-D), demonstrating that the availability of mesenchymal progenitors was unaffected. Next, we examined mesenchymal cell survival and proliferation at E12.5-E14.5. For analysis at E14.5, the elevated and non-elevated palatal shelves were analyzed independently in the asymmetric cases (Fig. 3L). We found no statistically significant difference in the number of apoptotic or proliferating cells at any stage (Fig. 3C-L, Fig. S2E-H). These results indicate that *Wnt1-Cre;Erk2*$^{fl/fl}$ palatal shelves did not have any intrinsic defect.

Because mutations affecting the mesenchyme can affect epithelial cells in a paracrine manner, we also checked whether the fate of the midline edge epithelium was compromised in *Wnt1-Cre;Erk2*$^{fl/fl}$ embryos. We cultured E13.5 palatal explants with the midlines placed in contact. After a 3-day incubation period, palatal fusion was complete and no remaining midline epithelial cells were detectable in either control or *Wnt1-Cre;Erk2*$^{fl/fl}$ explants (Fig. S3A,B). We also analyzed the AP patterning of the palatal epithelium by *in situ* hybridization of *Shh*, a marker that labels the rugae. The number and localization of rugae along the AP axis of the palates in E14.5 *Wnt1-Cre;Erk2*$^{fl/fl}$ mice were comparable to those of controls (Fig. S3C,D). These findings suggest that ERK pathway activation in the mesenchyme is not necessary for either the establishment of AP patterning or midline epithelial cell fate in the palate.

In order to understand the potential molecular causes underlying the palatal clefting in *Wnt1-Cre;Erk2*$^{fl/fl}$ mice, we carried out RNA microarray analysis of E13.5 and E14.5 palatal shelves, including both epithelium and mesenchyme. Despite the fact that ERK2 mediates a wide variety of extracellular signals, only a few genes were differentially expressed in the palates of mutants compared with those of controls at either stage (Tables S2 and S3). These genes do not appear to have any known functions in palatogenesis.

Development (2015) 142, 3734-3745 doi:10.1242/dev.125328

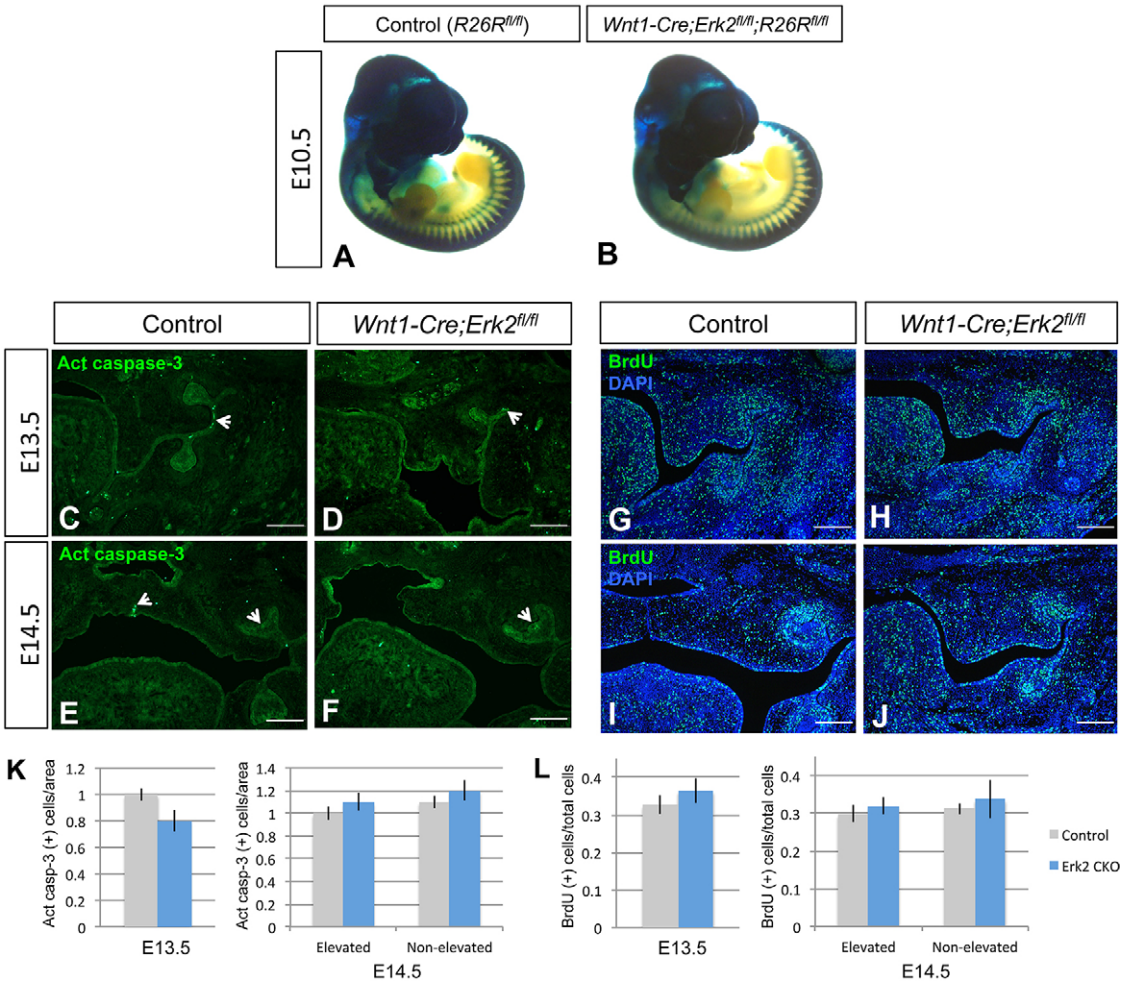

Fig. 3. Neural crest cell migration, cell survival, and proliferation of the palatal mesenchyme are unaffected in *Wnt1-Cre;Erk2^fl/fl^* mice. (A,B) *lacZ* staining of whole-mount E10.5 *Wnt1-Cre;R26R^fl/fl^* (control) and *Wnt1-Cre;Erk2^fl/fl^;R26R^fl/fl^* embryos. (C-F) Active caspase 3 immunostaining (green) of E13.5 and E14.5 control and *Wnt1-Cre;Erk2^fl/fl^* palates. Arrowheads indicate positive signal. (G-J) BrdU staining (green) of E13.5 and E14.5 control and *Wnt1-Cre;Erk2^fl/fl^* palates. (K,L) Quantification of apoptotic and proliferating cells in C-F and G-J, respectively. *n*=3. Scale bars: 100 µm.

Given the lack of significant molecular and cellular changes in *Wnt1-Cre;Erk2^fl/fl^* palates and the tight relationship between the phenotypes of palate, tongue and mandible, we hypothesized that the palatal clefting in these mice is a consequence of the malposition of the tongue and secondary to the mandibular defects. To test this hypothesis, we used both *in vivo* and *in vitro* approaches. First, we generated *Osr2-Cre;Erk2^fl/fl^* mice because *Osr2* is expressed in the palatal shelves from E12.5 to newborn stage but not in the mandible at any developmental stage (Parada et al., 2013; data not shown). Indeed, the expression of *Erk2* was reduced in the palatal shelves of *Osr2-Cre;Erk2^fl/fl^* mice, as indicated by qPCR analysis, whereas expression in the mandible was unaffected (Fig. 4A). Palatal clefting in these mice would suggest that ERK2 plays an intrinsic role in the elevation of the palatal shelves. However, *Osr2-Cre;Erk2^fl/fl^* newborns did not exhibit cleft palate (*n*=16; Fig. 4B-H). The tongues and mandibles in these mice were also unaffected (Fig. 4B-D).

Second, we performed *in vitro* experiments using a rotational culture system. The mandible and tongue were dissected at E13.5, before palatal shelf elevation, and at E14.0, immediately after elevation but before the palatal shelves make contact along the midline. After 3 days of culture, the palatal shelves from E13.5 control and *Erk2* mice were elevated although not fused, owing to technical limitations (*n*=4; Fig. 4I-L). Immunostaining for K14 and counterstaining with DAPI were performed to show the palatal epithelium and the integrity of the mesenchymal tissue. When dissected at E14.0 and cultured for 3 days, the palatal shelves of the control samples were fused at the midline, with no epithelial cells remaining in this region (*n*=3; Fig. 4M,O). Although *Wnt1-Cre;Erk2^fl/fl^* palatal shelves did not fuse, removing the tongue and mandible was sufficient to rescue the elevation defect (Fig. 4N,P). It is likely that fusion did not occur because of the previous delay in the elevation process. Taken together, these findings strongly suggest that the palatal shelf elevation defect in *Erk2* mutant mice is the result of a primary malformation in the tongue and/or mandible.

Proliferation and differentiation are unaffected in tongues of *Wnt1-Cre;Erk2^fl/fl^* mice

Tongues of *Wnt1-Cre;Erk2^fl/fl^* newborn mice exhibited microglossia, disruption of muscle patterning and malposition. We carefully examined cell survival, proliferation and differentiation in the tongue at different key stages. We found that cell survival was not affected in *Wnt1-Cre;Erk2^fl/fl^* tongues at E12.5 through E14.5 (Fig. S4). We evaluated cell proliferation separately in the muscular and neural crest-derived components using double immunostaining for Myod1, a marker of myogenic determination, and phosphohistone

Development (2015) 142, 3734-3745 doi:10.1242/dev.125328

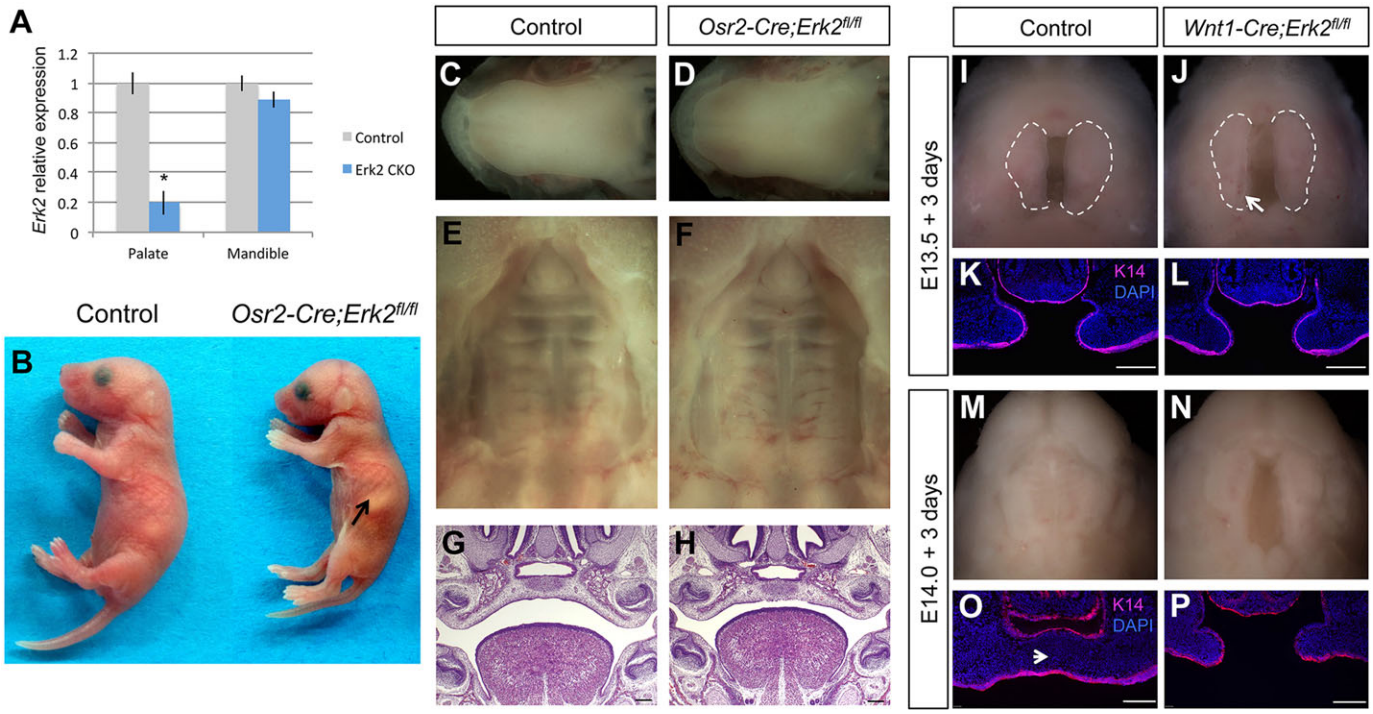

Fig. 4. Cleft palate is a consequence of tongue and mandible malformations in *Wnt1-Cre;Erk2$^{fl/fl}$* mice. (A) Quantitative analysis of *Erk2* expression in the palatal shelves and mandible of control and *Osr2-Cre;Erk2$^{fl/fl}$* mice at E13.5. *P<0.05. (B) Macroscopic views of control and *Osr2-Cre;Erk2$^{fl/fl}$* newborns. Arrow indicates milk in the stomach of the *Osr2-Cre;Erk2$^{fl/fl}$* mouse. (C-F) Intraoral views of the tongues, mandibles and palates of control and *Osr2-Cre;Erk2$^{fl/fl}$* newborns. (G,H) HE staining of coronal sections of E16.5 control and *Osr2-Cre;Erk2$^{fl/fl}$* mice. (I,J) Intraoral views of heads from E13.5 control and *Wnt1-Cre;Erk2$^{fl/fl}$* embryos from which the mandible and tongue were removed and cultured for 3 days (n=4). Dashed lines delineate the palatal shelves. (K,L) K14 immunostaining (red) of coronal sections of E13.5 cultured explants. (M,N). Intraoral views of heads from E14.0 control and *Wnt1-Cre;Erk2$^{fl/fl}$* embryos from which the mandible and tongue were removed and cultured for 3 days (n=3). (O,P) K14 immunostaining (red) of coronal sections of E14.0 cultured explants. Arrowhead in O points to the midline of the control sample, where palatal shelves are fused and no epithelial cells remain. Scale bars: 100 µm.

H3 (PH3), a marker of proliferation. Myod1-negative cells in the tongue correspond to the neural crest-derived mesenchyme. At E12.5 through E14.5, the numbers of proliferating cells in both the muscular and the neural crest components of the tongue were comparable in *Wnt1-Cre;Erk2$^{fl/fl}$* and control embryos (Fig. 5A-G). Next, we examined myogenic differentiation by analyzing the expression of myosin heavy chain (MHC), which labels mature muscle fibers. We detected no significant differences in the intensity of the signal between control and *Erk2* mutant tongues from E12.5 to E14.5 (Fig. 5H-M). Quantitative analysis of myogenin (*Myog*) and *Mrf4* (*Myf6*) expression at E13.5 and E14.5 also confirmed that muscle differentiation was unaffected in the tongues of *Wnt1-Cre;Erk2$^{fl/fl}$* embryos (Fig. 5N,O). Although no myogenic differentiation defects were detectable in *Erk2* mutant tongues, muscle patterning and organization were altered. Both microglossia and asymmetry in the tongue muscles, mainly affecting the extrinsic muscles, were detectable immediately before palatal shelf elevation at E13.5 (Fig. 5C,D,J,K, Fig. S5A,B). As development progressed, these phenotypes worsened and the patterns of both intrinsic and extrinsic muscles were severely disrupted by E14.5 (Fig. 5E,F,L,M, Fig. S5C,D). The stage of onset of the tongue extrinsic muscle asymmetry is consistent with the timing of the failure of palatal shelf elevation.

Next, we checked whether differentiation of neural crest-derived mesenchyme was affected in the tongues of *Wnt1-Cre;Erk2$^{fl/fl}$* mice by analyzing the expression of scleraxis (*Scx*). *Scx* is a marker for tendons, which are derived from neural crest cells in the craniofacial region. In control mice, *Scx* was expressed in the tongue septum and tendons of the extrinsic muscles at both E13.5 and E15.5. At E13.5, *Scx* expression was downregulated in *Wnt1-Cre;Erk2$^{fl/fl}$* tongues (Fig. 6A,B). At E15.5, *Scx* expression was completely undetectable in both the septum and tendons of *Erk2* mutant tongues (Fig. 6C,D). Type 1 collagen (*Col1a1*) was also undetectable in the tendons of the extrinsic muscles at this stage (data not shown). Because of the absence of tendons in *Wnt1-Cre;Erk2$^{fl/fl}$* tongues, we evaluated whether the relationship between the extrinsic muscles of the tongue and the mandibular bone primordium was affected by examining the expression of Sp7 (osterix), a marker for osteogenic progenitors, and MHC. At E13.5, Sp7 expression was significantly downregulated in *Wnt1-Cre;Erk2$^{fl/fl}$* mandibles (Fig. 6E,F, and see next section), which does not allow a proper comparison. At E15.5, the extrinsic muscles in control mice were not in contact with the Meckel's cartilage or the osteogenic progenitors, whereas they were attached directly to the cartilage and in close vicinity to the bone primordium in *Wnt1-Cre;Erk2$^{fl/fl}$* mice (Fig. 6G,H). We speculate that this abnormal relationship between muscles, cartilage and bone contributes to a mechanical disruption of tongue muscle development.

Based on the lack of intrinsic cellular defects in the tongue muscles and the correlation between the asymmetry and size of the mandible and tongue in *Wnt1-Cre;Erk2$^{fl/fl}$* mice, we hypothesized that the tongue malformation is a secondary defect. To address this issue, we performed *in vitro* experiments in which mandibles of E12.5 mice were removed and the tongue was cultured in isolation for 7 days. After this incubation period, macroscopic examination indicated that the sizes of control and *Wnt1-Cre;Erk2$^{fl/fl}$* tongues were similar (Fig. 7A). Next, we analyzed the volumes of cultured control and *Erk2* mutant tongues quantitatively using BioVis3D

Development (2015) 142, 3734-3745 doi:10.1242/dev.125328

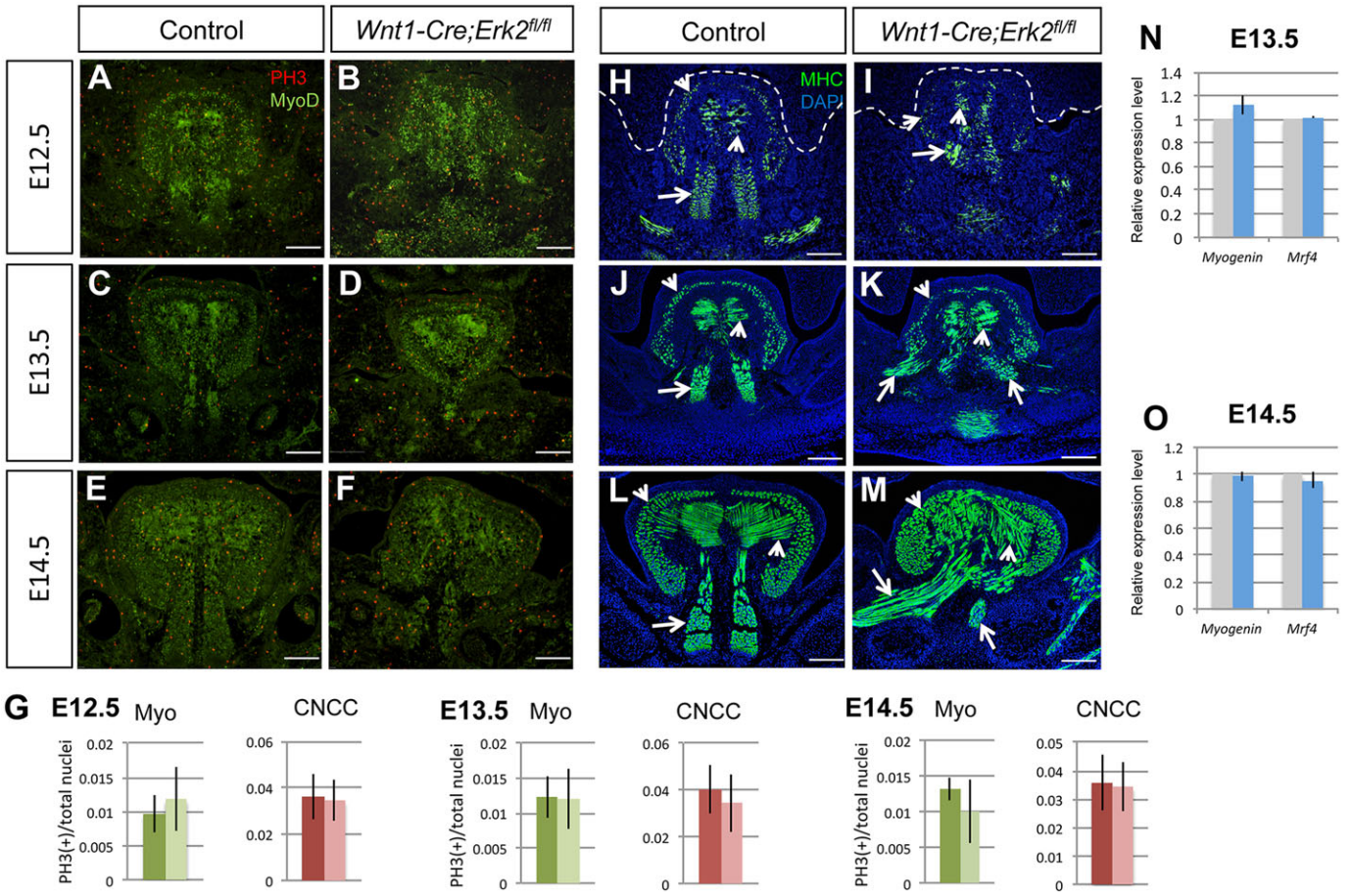

Fig. 5. Proliferation and differentiation are unaffected in *Wnt1-Cre;Erk2*$^{fl/fl}$ tongues. (A-F) PH3 (red) and Myod1 (green) double immunostaining of coronal sections of E12.5-E14.5 control and *Wnt1-Cre;Erk2*$^{fl/fl}$ tongues. (G) Quantification of proliferation (PH3^{+}) in Myod1-positive myogenic cells (Myo) and Myod1-negative cranial neural crest cells (CNCC) from A-F. Dark bars, control tongues; light bars, *Wnt1-Cre;Erk2*$^{fl/fl}$ tongues. (H-M) MHC immunostaining (green) of coronal sections of E12.5-E14.5 control and *Wnt1-Cre;Erk2*$^{fl/fl}$ tongues. Arrows point to the extrinsic muscles and arrowheads point to the intrinsic muscles. (N,O) Quantitation of real-time qPCR of *Myog* and *Mrf4* in control (gray bars) and *Wnt1-Cre;Erk2*$^{fl/fl}$ (blue bars) tongues at E13.5 and E14.5. *n*=3 for each stage and experiment. Scale bars: 100 µm.

software (*n*=4 and 3, respectively). Although the tongues of *Wnt1-Cre;Erk2*$^{fl/fl}$ mice were 16% smaller than those of controls after culture, statistical analysis showed that the difference was not significant (*P*=0.282; Fig. 7B). These findings suggest that the microglossia was considerably rescued upon removal of the mandible. Additionally, histological analyses and MHC immunostaining showed that the orientation and organization of muscle fibers of the intrinsic muscles of control and *Wnt1-Cre;Erk2*$^{fl/fl}$ tongues were comparable (Fig. 7C-F). The pattern and organization of the extrinsic muscles could not be evaluated using this approach. These results suggest that most of the phenotypes in *Wnt1-Cre;Erk2*$^{fl/fl}$ tongues were the consequence of a primary defect in the mandible.

Mandibular osteogenic differentiation is severely compromised in *Erk2* mutant mice

Based on our results, we suggest that *Wnt1-Cre;Erk2*$^{fl/fl}$ mice mimic human PRS, in which micrognathia leads to malposition of the tongue (glossoptosis), which blocks the elevation of the palatal shelves, eventually causing cleft palate (Movie 1). In order to study the primary defect in *Wnt1-Cre;Erk2*$^{fl/fl}$ mice, we performed a series of analyses of mandibles. 3D reconstruction of microCT scans at the newborn stage showed a ∼50% reduction in the mandibular volume of *Wnt1-Cre;Erk2*$^{fl/fl}$ mice, as well as obvious mandibular asymmetry (Fig. 8A,B,E,F,I). These findings were confirmed using skeletal staining. Remarkably, the proximal region of the mandible was severely affected whereas the defect in the distal region was mild. Specifically, the condyle was greatly reduced in size; the angle and the coronoid process were severely disrupted, or completely absent in some cases (Fig. 8A-H; data not shown). We collected embryos from E12.5 through E16.5 to determine the onset time of the mandibular malformations in *Wnt1-Cre;Erk2*$^{fl/fl}$ newborns. Micrognathia was detectable by E13.5 (Fig. 8J,K), which coincides with the appearance of the tongue defects. At E14.5, the mandibular phenotype was more severe (Fig. 8L,M), consistent with the increase in severity of the tongue defects. Moreover, the morphology of the Meckel's cartilage was disrupted at E14.5, with a reduction in size and a complete discontinuity on one side. The volume of mandibular bone was reduced, although the severity of this trait was not always correlated with the severity of the malformation of the Meckel's cartilage (Fig. 8N-Q).

In order to determine the cause(s) of the mandibular defects in *Wnt1-Cre;Erk2*$^{fl/fl}$ mice, we analyzed potential cellular activities that could be affected from E12.5 to E15.5. Cell proliferation and survival in the mandibles of *Wnt1-Cre;Erk2*$^{fl/fl}$ mice were indistinguishable from controls at all time points (Fig. 9A-D; data not shown). Because the morphology of the Meckel's cartilage was affected, we examined the expression of several chondrogenesis

Development (2015) 142, 3734-3745 doi:10.1242/dev.125328

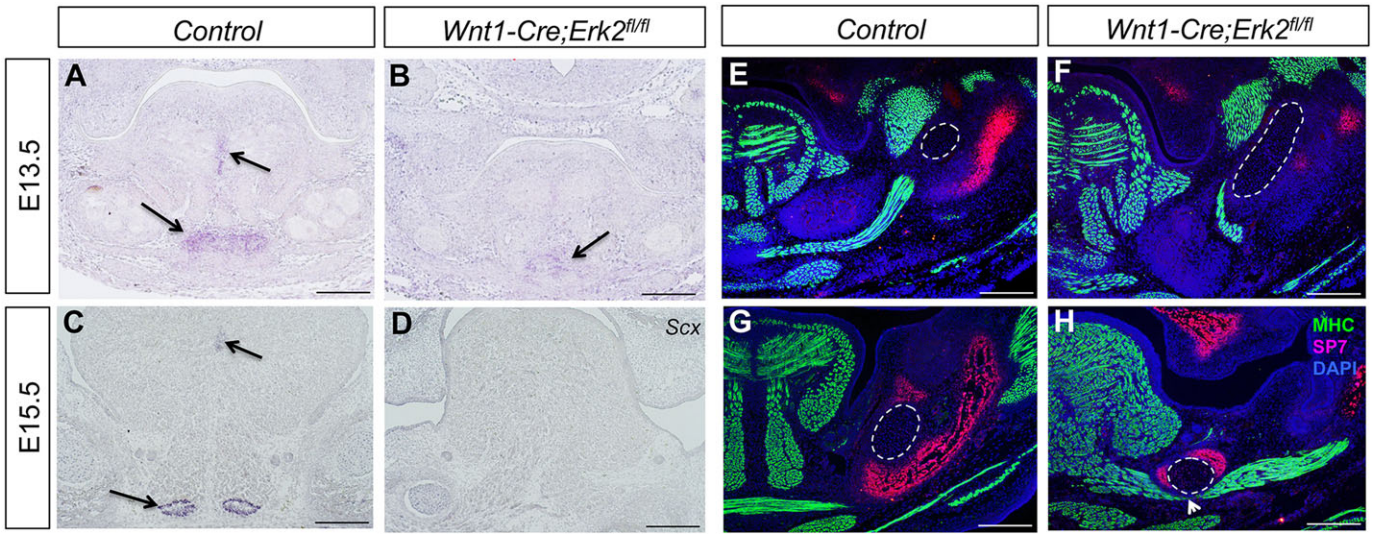

Fig. 6. Cranial neural crest cell-derived tendons are abnormal in *Wnt1-Cre;Erk2*$^{fl/fl}$ tongues. (A-D) *In situ* hybridization of scleraxis (*Scx*) in coronal sections of E13.5 and E15.5 control and *Wnt1-Cre;Erk2*$^{fl/fl}$ heads. Arrows indicate *Scx* expression. (E-H) Double immunostaining of Sp7 (red) and MHC (green) in coronal sections of E13.5 and E15.5 control and *Wnt1-Cre;Erk2*$^{fl/fl}$ heads. Dashed lines delineate the Meckel's cartilage. The arrowhead in H indicates the abnormally close proximity of the extrinsic muscles of the tongue to the Meckel's cartilage and osteogenic progenitors. *n*=3 for each stage and analysis. Scale bars: 100 µm.

markers. Expression of *Sox9* and Link protein is detectable in most chondroblasts in the Meckel's cartilage of control embryos (Fig. 9E, Fig. S6A,E; data not shown). Surprisingly, in *Wnt1-Cre;Erk2*$^{fl/fl}$ mandibles at E13.5 and E14.5, the expression of these markers was comparable to that of controls in both intensity and pattern, although there was a significant difference in shape and size of the cartilage (Fig. 9E,F, Fig. S6A,B,E,F). Similarly, *Ctgf* was expressed in the peripheral chondroblasts of the Meckel's cartilage of both control and *Wnt1-Cre;Erk2*$^{fl/fl}$ mice (Fig. S6C,D,G,H).

Next, we examined the expression of two osteogenic differentiation markers. Sp7 is a marker for osteogenic progenitors and type 1 collagen (*Col1a1*) is a marker for terminally differentiated osteoblasts. We first analyzed embryos at E13.5, which corresponds to the onset of the mandibular defects in *Wnt1-Cre;Erk2*$^{fl/fl}$ mice. At this stage, when deposition of osteogenic matrix is first detectable in control mandibles, Sp7 expression was dramatically downregulated and *Col1a1* expression was undetectable in the mandibular primordium of *Wnt1-Cre;Erk2*$^{fl/fl}$ mice (Fig. 9H-K). We also checked other developmental stages, before and after the beginning of mandibular osteogenic differentiation. At E12.5, *Col1a1* was not expressed in controls (data not shown) and Sp7 was detectable in the condensed mesenchyme neighboring the Meckel's cartilage. In *Wnt1-Cre;Erk2*$^{fl/fl}$ mice, the number of Sp7-positive cells was reduced, suggesting that the availability of osteogenic progenitors was compromised (Fig. S7A,B). At E14.5 and E15.5, the domains expressing either Sp7 or *Col1a1* were reduced in an asymmetric pattern in *Wnt1-Cre;Erk2*$^{fl/fl}$ mice (Fig. S7C-J). These data indicate that there is an initial decrease in the pool of osteogenic progenitors followed by a significant delay in the osteogenic process, which results in a small, asymmetric mandible in *Wnt1-Cre;Erk2*$^{fl/fl}$ mice.

DISCUSSION

In this work we have investigated the function of the ERK/MAPK transduction pathway in the postmigratory neural crest cells populating the craniofacial region. *Wnt1-Cre;Erk2*$^{fl/fl}$ mice exhibit severe craniofacial malformations that mimic human PRS, which is characterized by a primary mandibular defect that causes malposition of the tongue and consequently cleft palate. Similarly, the cleft palate in *Wnt1-Cre;Erk2*$^{fl/fl}$ mice is not the primary defect, but is instead the result of defects in the mandible that affect the tongue and eventually the formation of the palate. Accordingly, the ERK/MAPK pathway is active in mesenchymal progenitors committed to the osteogenic mesenchyme and regulates early steps in the osteogenic differentiation program in the mandibular primordium, which appears to be essential for the proper size and morphology of the mandible.

Failure of palatal shelf elevation and expression of PRS phenotypes in *Wnt1-Cre;Erk2*$^{fl/fl}$ mice

Elevation of the palatal shelves is a complex process that depends on both intrinsic and extrinsic factors. Our results highlight the relevance of extrinsic influences for palatal shelf elevation. Among them, the cranial base and mandible have been the focus of numerous studies. As the palatal shelves elevate, the cranial base cartilage straightens significantly. One theory speculates that this straightening generates forces in the midline that are transmitted to the alar regions of the sphenoid and then to the palatal shelves during elevation (Brinkley and Vickerman, 1978). In *Wnt1-Cre;Erk2*$^{fl/fl}$ mice the cranial base is not affected (data not shown), but mandibular morphology is severely disrupted. In wild-type mice, the mandibular primordium grows downward and lengthens from E12.5 to newborn stage (Ramaesh and Bard, 2003). This growth pattern seems to provide the tongue with physical space to move downward, and this movement closely coincides with the reorientation of the palatal shelves from a vertical to a horizontal position. The lack of mandibular growth in *Wnt1-Cre;Erk2*$^{fl/fl}$ mice diminishes the space available for the tongue to descend. Subsequently, the high position of the tongue (glossoptosis) blocks palatal shelf elevation.

Loss of *Erk2* in the neural crest-derived mesenchyme also affects the size of the tongue. Similar cases of microglossia occur in other mouse models with mesenchymal mutations, such as *Wnt1-Cre;Tgfbr2*$^{fl/fl}$ (Hosokawa et al., 2010; Iwata et al., 2013) and *Wnt1-Cre;Alk5*$^{fl/fl}$ (Han et al., 2014) mice. However, in those cases, changes in molecules secreted by the mesenchymal cells directly affect the tongue myogenic progenitors, resulting in altered myogenic

Development (2015) 142, 3734-3745 doi:10.1242/dev.125328

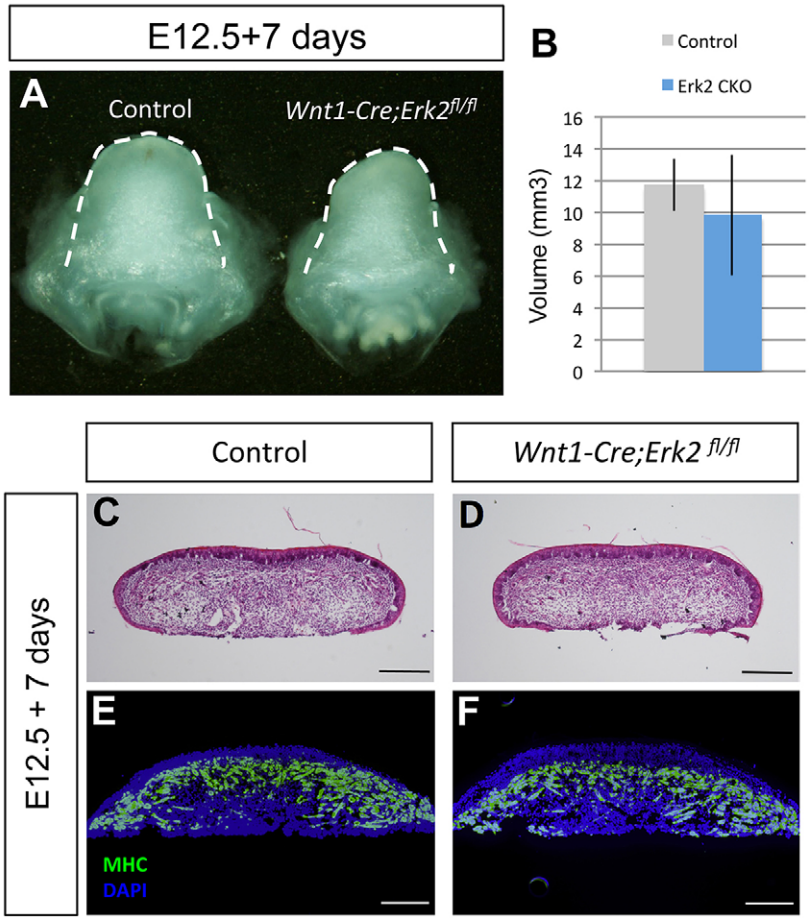

Fig. 7. Tongue defects in *Wnt1-Cre;Erk2*$^{fl/fl}$ mice are secondary to micrognathia. (A) Macroscopic view of tongue explants from control and *Wnt1-Cre;Erk2*$^{fl/fl}$ embryos after 7 days of culture. Dashed lines delineate the tongue. (B) Volume analyses of cultured control and *Wnt1-Cre;Erk2*$^{fl/fl}$ tongues (n=4 and n=3, respectively). (C-F) HE staining (C,D) and MHC immunostaining (E,F; green) of coronal sections of tongue explants cultured for 7 days. n=4. Scale bars: 200 µm.

proliferation and/or differentiation. In *Wnt1-Cre;Erk2*$^{fl/fl}$ mice, the proliferation, survival and differentiation of the myogenic precursors are unaffected, suggesting that mechanical restriction produced by the small mandible plays a major role in the tongue phenotype. The misorientation of the tongue muscles in *Wnt1-Cre;Erk2*$^{fl/fl}$ mice is consistent with the asymmetry of the mandible, and the onsets of the macroscopic defects in the tongue and mandible coincide. Furthermore, the septum and tendons for the extrinsic muscles of the tongue are affected in *Wnt1-Cre;Erk2*$^{fl/fl}$ mice; consequently, the insertion of these muscles into the mandible is abnormal. This feature may be independent of the defect in mandibular osteogenesis or linked to it, but either way it might alter the distribution of mechanical forces and contribute to the malposition of the tongue. Unfortunately, it is not possible to assess its influence with the techniques currently available. To examine the intrinsic function of the ERK pathway in the muscular component of the tongue, we also generated *Myf5-Cre;Erk2*$^{fl/fl}$ mice. These mice did not display any malformation affecting the tongue (data not shown), which highlights the importance of the ERK pathway in neural crest-derived structures for the correct patterning and organization of tongue muscles.

Several previous studies have reported the failure of palate elevation due to physical obstruction by the tongue in mice (Huang et al., 2008; Song et al., 2013). However, only mutation of *Prdm16* causes failed palate elevation associated with a highly positioned tongue and smaller mandibular bone, mimicking human PRS (Bjork et al., 2010) and similar to *Wnt1-Cre;Erk2*$^{fl/fl}$ mice. Still, there is no direct evidence to show that the cleft palate in *Prdm16* mutant mice is due to the mandibular malformation. *ActRcII*-deficient mice, which lack activin type II receptor (Acvr2), also show skeletal and facial abnormalities reminiscent of PRS but with very low penetrance (Matzuk et al., 1995). Here we present an animal model with 100% phenotype penetrance, ideal for the analysis of this developmental disorder with the ultimate goal of elucidating its pathogenesis and generating preventive approaches and/or early and more effective therapies. This is relevant from a clinical perspective because PRS in humans has a relatively high incidence of 1:8500-14,000 live births and it frequently leads to life-threatening obstructive apnea and feeding difficulties during the neonatal period (Tan et al., 2013).

The role of ERK/MAPK in mandibular osteogenesis

A number of human syndromes result from mutations in diverse members of the ERK/MAPK cascade (Aoki et al., 2008; Narumi et al., 2007; Newbern et al., 2008; Roberts et al., 2006). All of these syndromes display various skeletal manifestations, including short stature and craniofacial and limb abnormalities (Aoki et al., 2008; Narumi et al., 2007; Newbern et al., 2008; Roberts et al., 2006). In this work, we have shown that ablation of the ERK pathway in neural crest derivatives leads to a severe defect in osteogenic differentiation in the mandible. Although our results suggest that the ERK pathway is active in specific domains of the palate, tongue and mandible at different developmental stages, the phenotype of *Wnt1-Cre;Erk2*$^{fl/fl}$ mice indicates a differential requirement for this pathway in these structures. Similarly, *Srf* mutant mice display fully penetrant mandibular hypoplasia but their maxillary hypoplasia is less severe than that of *Wnt1-Cre;Erk2*$^{fl/fl}$ mice and the tongue is not affected (Newbern et al., 2008). Srf is a downstream target of the

Development (2015) 142, 3734-3745 doi:10.1242/dev.125328

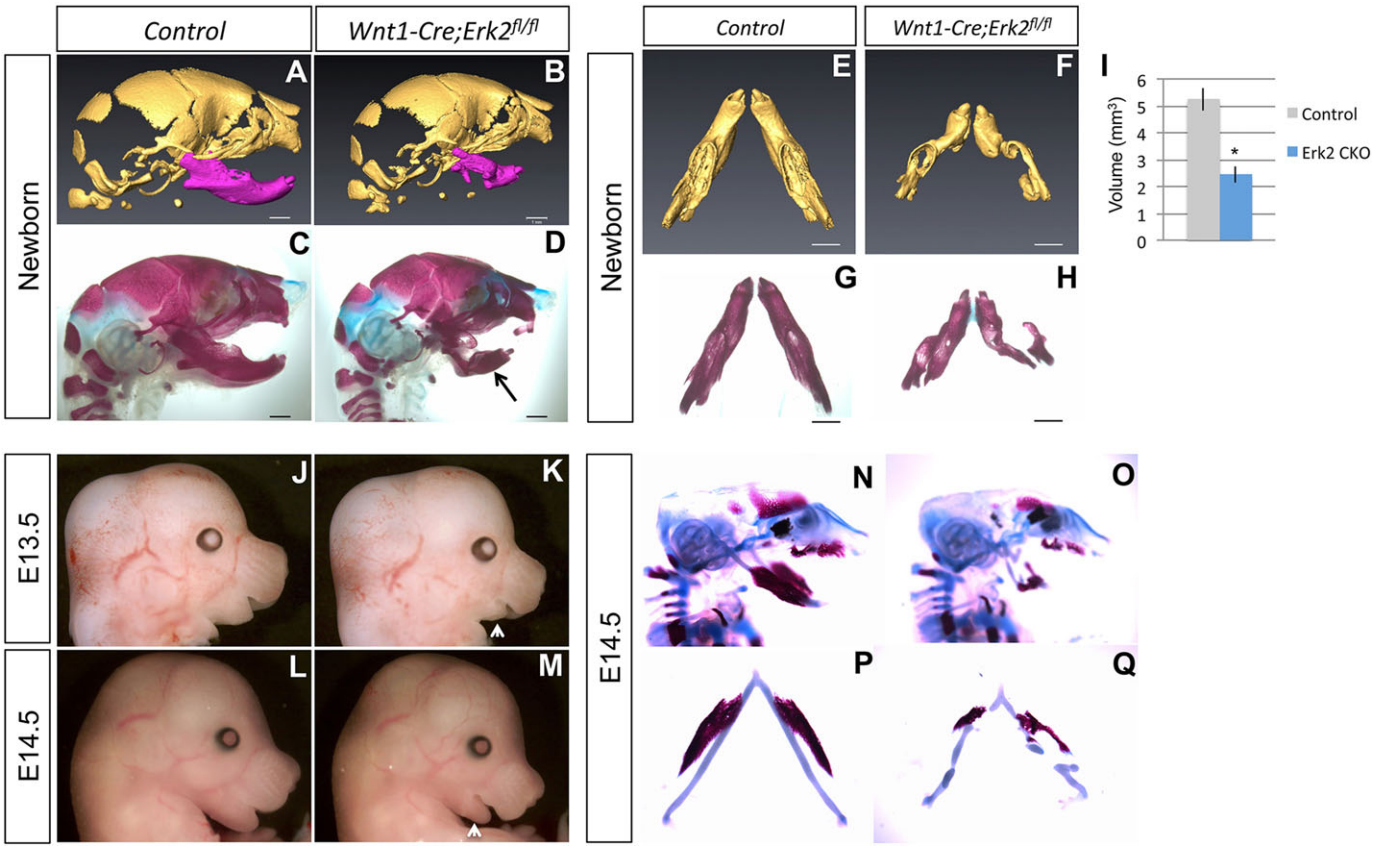

Fig. 8. The onset of mandibular defects precedes palatal shelf elevation. (A-D) Sagittal views of 3D reconstructions from microCT scans (A,B) and Alizarin Red/Alcian Blue staining (C,D) of newborn control and *Wnt1-Cre;Erk2*$^{fl/fl}$ skulls. Arrow in D points to the malformed mandible in *Erk2* mutant mice. (E-H) Intraoral views of 3D reconstructions from microCT scans (E,F) and Alizarin Red/Alcian Blue staining (G,H) of newborn control and *Wnt1-Cre;Erk2*$^{fl/fl}$ mandibles. (I) Quantification of the volume of control and *Wnt1-Cre;Erk2*$^{fl/fl}$ mandibles from 3D reconstructions. **P*<0.05. (J-M) Macroscopic sagittal views of E13.5 and E14.5 control and *Wnt1-Cre;Erk2*$^{fl/fl}$ embryos. Arrowheads indicate malformed mandibles. (N-Q) Skeletal staining of skulls and mandibles from E14.5 control and *Wnt1-Cre;Erk2*$^{fl/fl}$ embryos. *n*=3 for each stage. Scale bars: 1 mm.

ERK pathway, which acts through the ternary complex factors (Dalton et al., 1993). Therefore, we speculate that the high sensitivity of the mandible to loss of *Erk2* is due to a lack of functional redundancy with other members of the pathway and/or to the expression of a different set of transcriptional downstream targets compared with the palate or tongue.

Mandibular bone formation occurs via intramembranous ossification, in which mesenchymal cells differentiate directly into osteoblasts (Orliaguet et al., 1993). Previous *in vitro* and *in vivo* studies have shown that the ERK pathway is involved in the regulation of both endochondral and intramembranous ossification processes (Chen et al., 2014; Kyono et al., 2012). For example, *Prx1-Cre;Erk1*$^{-/-}$*;Erk2*$^{fl/fl}$ mice exhibit defective bone formation in their limbs and calvaria, which is mainly caused by a disruption of the osteoblast differentiation program after Runx2, Sp7 and Atf4 expression and before osteocalcin (Bglap) expression. In addition, ectopic cartilage was formed in these mice (Matsushita et al., 2009). *Prx1-Cre;Erk1*$^{-/-}$*;Erk2*$^{fl/fl}$ mice exhibit no mandibular defects, probably because only a subset of neural crest cells was affected. In *Wnt1-Cre;Erk2*$^{fl/fl}$ mice, the expression of master transcription factors such as Sp7 and Runx2 was severely downregulated in the mandibular primordium (data not shown), suggesting that the ERK pathway is involved in the regulation of early steps in the osteogenic differentiation program. Specifically, ERK activation might define the pool of osteogenic progenitors in the mandible that will differentiate into osteoblasts but is unlikely to be involved at later stages of osteoblast differentiation. This model is based on the activation pattern of the ERK pathway, in which P-ERK is detectable in mesenchymal cells that are committed to the osteogenic lineage but disappears at later stages in differentiated *Col1a1*-positive osteoblasts. In contrast to our data, late effects of the ERK pathway on osteoblast differentiation have been reported in limbs and calvarial bone (Ge et al., 2007; Kyono et al., 2012). Further analyses of downstream molecular events in *Wnt1-Cre;Erk2*$^{fl/fl}$ mice are needed to understand the functional mechanism of the ERK pathway during mandible bone development.

MATERIALS AND METHODS

Generation of transgenic mice

Mating *Wnt1-Cre;Erk2*$^{fl/+}$ mice with *Erk2*$^{fl/fl}$ or *Erk2*$^{fl/fl}$*;R26R*$^{fl/fl}$ mice generated *Wnt1-Cre;Erk2*$^{fl/fl}$ and *Wnt1-Cre;Erk2*$^{fl/fl}$*;R26R*$^{fl/+}$ mice, respectively. *Osr2-Cre;Erk2*$^{fl/+}$ mice were crossed with *Erk2*$^{fl/fl}$ mice to generate *Osr2-Cre;Erk2*$^{fl/fl}$ mice. Animal usage was approved by the Institutional Animal Care and Use Committee (IACUC) at the University of Southern California.

MicroCT scanning and 3D reconstruction

Control and *Wnt1-Cre;Erk2*$^{fl/fl}$ newborn mice were sacrificed and heads were fixed in 4% paraformaldehyde (PFA). The skulls were imaged using a microCT system (Scanco Medical_V1.2a) as previously described (Parada et al., 2013). Visualization and 3D microCT reconstruction of the skull were performed using Isosurface parameters in Avizo 7 (Visualization Sciences Group).

Development (2015) 142, 3734-3745 doi:10.1242/dev.125328

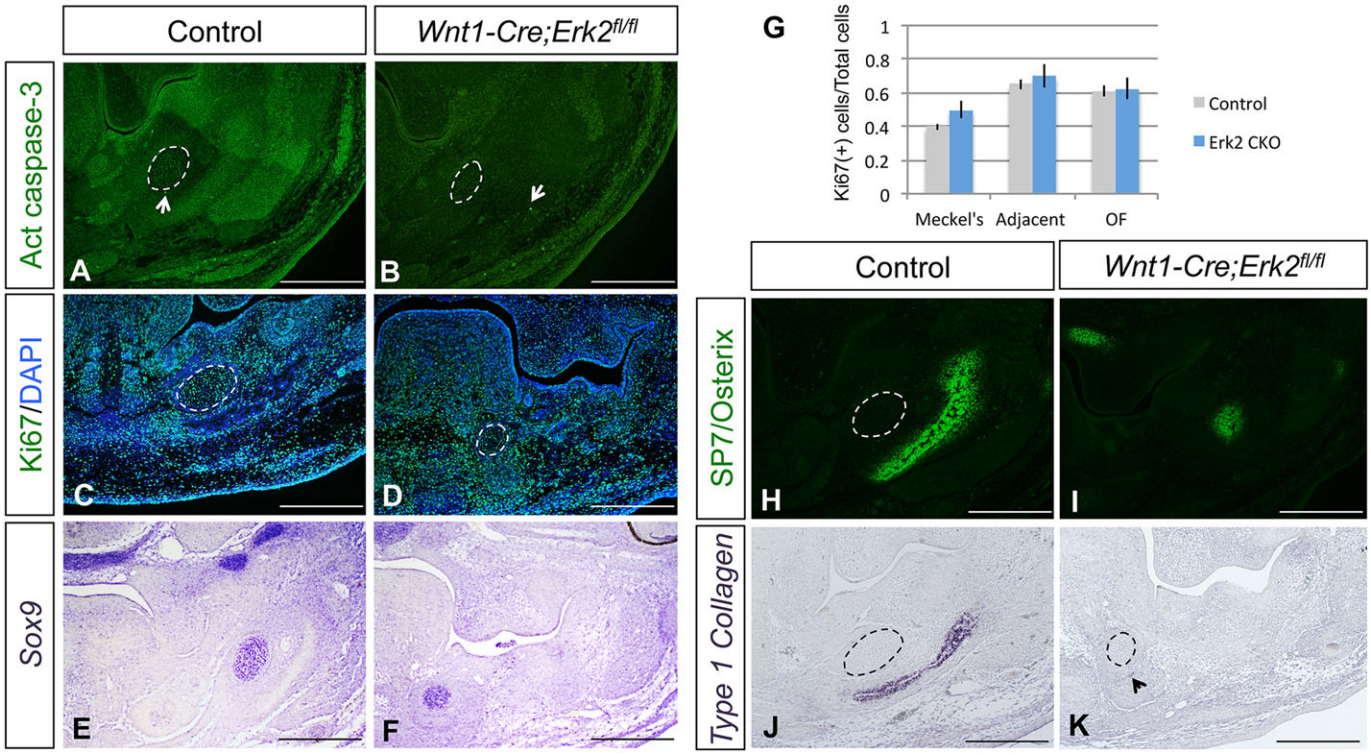

Fig. 9. Osteogenic differentiation is compromised in *Wnt1-Cre;Erk2*$^{fl/fl}$ mandibles. (A-D) Active caspase 3 (A,B; green) and Ki67 (C,D; green) immunostaining of control and *Wnt1-Cre;Erk2*$^{fl/fl}$ mandibles. Arrowheads indicate apoptotic cells. (E,F) *Sox9 in situ* hybridization of control and *Wnt1-Cre;Erk2*$^{fl/fl}$ embryos. (G) Quantification from C,D of proliferating cells in three different areas of the mandible: Meckel's cartilage, adjacent mesenchyme, and the osteogenic front (OF). (H-K) Sp7 immunostaining and type 1 collagen (*Col1a1*) *in situ* hybridization of control and *Wnt1-Cre;Erk2*$^{fl/fl}$ mandibles. Arrowhead indicates weak expression of *Col1a1*. Dashed lines delineate the Meckel's cartilage. *n*=3 for each analysis. Scale bars: 200 µm.

Skeletal staining

Skeletal staining of the skull of *Wnt1-Cre;Erk2*$^{fl/fl}$ and control mice was performed using a modified Alcian Blue-Alizarin Red S staining protocol. Briefly, newborns were fixed in 4% PFA, followed by a 1 h wash in double-distilled (dd) H_2O and post-fixation in 70% ethanol. The skin and internal organs were removed. The skeletons were stained with 0.02% Alcian Blue 8GX for 2 days. The samples were washed with ethanol/glacial acetic acid (7:3) for 1 h. Then, they were soaked in 100% ethanol overnight and then in ddH_2O for 1 day. Once the cartilage was detectable, Alizarin Red staining was performed overnight. Finally, the samples were treated with a KOH/glycerol series and stored in glycerol.

Histological analysis

For general morphology, deparaffinized sections were stained with Hematoxylin and Eosin (HE) using standard procedures. X-gal staining and detection of β-galactosidase (β-gal) activity in whole-mount embryos and tissue sections were performed as previously described (Chai et al., 2000).

Organ culture of palates

Timed-pregnant mice were sacrificed at E13.5. The palatal shelves of the embryos were microdissected and cultured in serum-free chemically defined medium as previously described (Ito et al., 2003). To test epithelial degeneration and fusion, palatal shelves were placed in contact at the midline and cultured for 3 days. Then, they were fixed in 4% PFA and prepared for histology and immunostaining.

Organ culture of tongues and volumetric analysis

Timed-pregnant mice were sacrificed at E12.5. The tongues of the embryos were microdissected and cultured in serum-free chemically defined medium as previously described for the culture of palatal explants (Ito et al., 2003). Tongues were cultured for 7 days. Then, they were fixed in 4% PFA and prepared for histology and immunostaining. 3D reconstruction and volumetric analyses were performed using BioVis3D software.

Rotational explant culture

Timed-pregnant mice were sacrificed at E13.5 and decapitated in PBS. The mandibles and tongues were removed from the embryos and each explant including the upper two-thirds of the head was placed in a 50-ml Falcon tube containing 5 ml BGJb (Gibco, 12591) supplemented with 50% fetal bovine serum and antibiotics. Tubes were placed in a rotary apparatus rotating at 50 rpm in an incubator at 37°C and 5% CO_2. After 3 days in culture, the explants were fixed in 4% PFA and processed.

BrdU incorporation and immunohistochemistry

Cell proliferation within the palate was monitored by intraperitoneal 5-bromo-2′-deoxyuridine (BrdU, Sigma) injection (100 µg/g body weight) at E12.5, E13.5 and E14.5. Two hours after injection, mice were sacrificed and embryos were fixed in 4% PFA and processed for immunohistochemistry. Detection of BrdU-labeled cells in E13.5 and E14.5 embryos was carried out using an antibody to BrdU followed by incubation with a fluorescent antibody. The BrdU Labeling and Detection Kit (Boehringer Mannheim) was used to process E12.5 samples. Other antibodies used for immunohistochemistry included myosin heavy chain (MHC; DSHB; 1:10), active caspase 3 (Abcam, ab2302; 1:100), K14 (Santa Cruz Biotechnology, sc-17104; 1:25), Ki67 (Abcam, ab15580; 1:100), Link protein (DSHB; 1:25), Myod1 (Abcam, ab203383; 1:50), phosphohistone H3 (PH3; Millipore, 06-570; 1:100), SP7/osterix (Abcam, ab22552; 1:100) and P-ERK1/2 (Cell Signaling Technology, 4370; 1:25). Alexa Fluor 488 and 594 fluorescent secondary antibodies (Invitrogen Life Technologies; 1:400) were used. Sections were counterstained with DAPI and imaged by fluorescence microscopy.

Development (2015) 142, 3734-3745 doi:10.1242/dev.125328

In situ hybridization

The expression patterns of *Shh*, *Sox9* and *Col1a1* were examined by *in situ* hybridization using digoxigenin-labeled antisense probes following standard procedures (Wilkinson, 1992; Xu et al., 2005). Paraffinized sections or dissected palatal shelves were used.

Microarray analysis

Total RNA samples (1 µg per sample) were converted into biotin-labeled cRNA using the GeneChip IVT Labeling Kit and standard protocols recommended by Affymetrix. Fragmented cDNA was applied to GeneChip Mouse Genome 430 2.0 Arrays (Affymetrix) that contain probe sets designed to detect over 45,000 transcripts. Microarrays were hybridized, processed and scanned as previously described using the manufacturer's recommended conditions. The R/Bioconductor software suite was used to generate scaled $\log_2$ transformed gene expression values using the GCRMA algorithm. Differential expression of transcripts was evaluated using a moderated *t*-test and *P*-values calculated by the limma Bioconductor package (Smyth et al., 2005). The false discovery rate (FDR) was estimated using the SPLOSH (spacings LOESS histogram) method. Transcripts showing >1.5-fold differential expression with a <5% FDR were identified as differentially expressed. All scaled gene expression scores and .cel files are available at the National Center for Biotechnology Information (NCBI) Gene Expression Omnibus (GEO) repository under series accession number GSE67087.

Quantitative (q) PCR analysis

Total RNA was isolated from dissected tissues using the RNeasy Mini Kit (Qiagen). The QuantiTect Reverse Transcription Kit (Qiagen) was used for cDNA synthesis. qPCR was carried out on an iCycler (Bio-Rad) with gene-specific primers and SYBR Green (Bio-Rad). Values were normalized to *Gapdh*.

Statistical analysis

Two-tailed Student's *t*-tests were applied for statistical analysis. For all graphs, data are represented as mean±s.d. $P<0.05$ was considered statistically significant.

Acknowledgements

We thank Drs Julie Mayo and Bridget Samuels for critical reading of the manuscript and Dr Gary E. Landreth for providing *Erk2*$^{fl/fl}$ mice.

Competing interests

The authors declare no competing or financial interests.

Author contributions

C.P. and Y.C. designed experiments and analyzed data. C.P., D.H., A.G. and P.S. performed the experiments. R.P. analyzed the microarray data. S.S.P. prepared the microCT images and 3D reconstructions. P.A.S-L. contributed to the discussion of the results. C.P. and Y.C. wrote the paper.

Funding

This study was supported by grants from the National Institute of Dental and Craniofacial Research, National Institutes of Health [R01DE012711 and U01DE020065] to Y.C. Deposited in PMC for release after 12 months.

Supplementary information

Supplementary information available online at
http://dev.biologists.org/lookup/suppl/doi:10.1242/dev.125328/-/DC1

References

Aoki, Y., Niihori, T., Narumi, Y., Kure, S. and Matsubara, Y. (2008). The RAS/MAPK syndromes: novel roles of the RAS pathway in human genetic disorders. *Hum. Mutat.* **29**, 992-1006.

Bjork, B. C., Turbe-Doan, A., Prysak, M., Herron, B. J. and Beier, D. R. (2010). Prdm16 is required for normal palatogenesis in mice. *Hum. Mol. Genet.* **19**, 774-789.

Brinkley, L. L. and Vickerman, M. M. (1978). The mechanical role of the cranial base in palatal shelf movement: an experimental re-examination. *J. Embryol. Exp. Morphol.* **48**, 93-100.

Bush, J. O. and Jiang, R. (2012). Palatogenesis: morphogenetic and molecular mechanisms of secondary palate development. *Development* **139**, 231-243.

Chai, Y. and Maxson, R. E., Jr. (2006). Recent advances in craniofacial morphogenesis. *Dev. Dyn.* **235**, 2353-2375.

Chai, Y., Jiang, X., Ito, Y., Bringas, P., Jr, Han, J., Rowitch, D. H., Soriano, P., McMahon, A. P. and Sucov, H. M. (2000). Fate of the mammalian cranial neural crest during tooth and mandibular morphogenesis. *Development* **127**, 1671-1679.

Chen, Z., Yue, S. X., Zhou, G., Greenfield, E. M. and Murakami, S. (2014). ERK1 and ERK2 regulate chondrocyte terminal differentiation during endochondral bone formation. *J. Bone Miner. Res.* **30**, 765-774.

Corson, L. B., Yamanaka, Y., Lai, K.-M. and Rossant, J. (2003). Spatial and temporal patterns of ERK signaling during mouse embryogenesis. *Development* **130**, 4527-4537.

Dalton, S., Marais, R., Wynne, J. and Treisman, R. (1993). Isolation and characterization of SRF accessory proteins. *Philos. Trans. R. Soc. Lond. B Biol. Sci.* **340**, 325-332.

Ferguson, M. W. J. (1977). The mechanism of palatal shelf elevation and the pathogenesis of cleft palate. *Virchows Arch. A Pathol. Anat. Histol.* **375**, 97-113.

Ferguson, M. W. (1988). Palate development. *Development* **103** Suppl, 41-60.

Ge, C., Xiao, G., Jiang, D. and Franceschi, R. T. (2007). Critical role of the extracellular signal-regulated kinase-MAPK pathway in osteoblast differentiation and skeletal development. *J. Cell Biol.* **176**, 709-718.

Han, A., Zhao, H., Li, J., Pelikan, R. and Chai, Y. (2014). ALK5-mediated transforming growth factor β signaling in neural crest cells controls craniofacial muscle development via tissue-tissue interactions. *Mol. Cell. Biol.* **34**, 3120-3131.

Hosokawa, R., Oka, K., Yamaza, T., Iwata, J., Urata, M., Xu, X., Bringas, P., Jr, Nonaka, K. and Chai, Y. (2010). TGF-beta mediated FGF10 signaling in cranial neural crest cells controls development of myogenic progenitor cells through tissue–tissue interactions during tongue morphogenesis. *Dev. Biol.* **341**, 186-195.

Huang, X., Goudy, S. L., Ketova, T., Litingtung, Y. and Chiang, C. (2008). Gli3-deficient mice exhibit cleft palate associated with abnormal tongue development. *Dev. Dyn.* **237**, 3079-3087.

Ito, Y., Yeo, J. Y., Chytil, A., Han, J., Bringas, P., Jr, Nakajima, A., Shuler, C. F., Moses, H. L. and Chai, Y. (2003). Conditional inactivation of Tgfbr2 in cranial neural crest causes cleft palate and calvaria defects. *Development* **130**, 5269-5280.

Iwata, J., Parada, C. and Chai, Y. (2011). The mechanism of TGF-β signaling during palate development. *Oral Dis.* **17**, 733-744.

Iwata, J.-i., Suzuki, A., Pelikan, R. C., Ho, T.-V. and Chai, Y. (2013). Noncanonical transforming growth factor β (TGFβ) signaling in cranial neural crest cells causes tongue muscle developmental defects. *J. Biol. Chem.* **288**, 29760-29770.

Kyono, A., Avishai, N., Ouyang, Z., Landreth, G. E. and Murakami, S. (2012). FGF and ERK signaling coordinately regulate mineralization-related genes and play essential roles in osteocyte differentiation. *J. Bone Miner. Metab.* **30**, 19-30.

Matsushita, T., Chan, Y. Y., Kawanami, A., Balmes, G., Landreth, G. E. and Murakami, S. (2009). Extracellular signal-regulated kinase 1 (ERK1) and ERK2 play essential roles in osteoblast differentiation and in supporting osteoclastogenesis. *Mol. Cell. Biol.* **29**, 5843-5857.

Matzuk, M. M., Kumar, T. R. and Bradley, A. (1995). Different phenotypes for mice deficient in either activins or activin receptor type II. *Nature* **374**, 356-360.

Melkoniemi, M., Koillinen, H., Mannikko, M., Warman, M. L., Pihlajamaa, T., Kääriäinen, H., Rautio, J., Hukki, J., Stofko, J. A., Cisneros, G. J. et al. (2003). Collagen XI sequence variations in nonsyndromic cleft palate, Robin sequence and micrognathia. *Eur. J. Hum. Genet.* **11**, 265-270.

Narumi, Y., Aoki, Y., Niihori, T., Neri, G., Cavé, H., Verloes, A., Nava, C., Kavamura, M. I., Okamoto, N., Kurosawa, K. et al. (2007). Molecular and clinical characterization of cardio-facio-cutaneous (CFC) syndrome: overlapping clinical manifestations with Costello syndrome. *Am. J. Med. Genet. A* **143A**, 799-807.

Newbern, J., Zhong, J., Wickramasinghe, R. S., Li, X., Wu, Y., Samuels, I., Cherosky, N., Karlo, J. C., O'Loughlin, B., Wikenheiser, J. et al. (2008). Mouse and human phenotypes indicate a critical conserved role for ERK2 signaling in neural crest development. *Proc. Natl. Acad. Sci. USA* **105**, 17115-17120.

Orliaguet, T., Dechelotte, P., Scheye, T. and Vanneuville, G. (1993). The relationship between Meckel's cartilage and the development of the human fetal mandible. *Surg. Radiol. Anat.* **15**, 113-118.

Parada, C., Li, J., Iwata, J., Suzuki, A. and Chai, Y. (2013). CTGF mediates Smad-dependent transforming growth factor β signaling to regulate mesenchymal cell proliferation during palate development. *Mol. Cell. Biol.* **33**, 3482-3493.

Pearson, G., Robinson, F., Beers Gibson, T., Xu, B. E., Karandikar, M., Berman, K. and Cobb, M. H. (2001). Mitogen-activated protein (MAP) kinase pathways: regulation and physiological functions. *Endocr. Rev.* **22**, 153-183.

Ramaesh, T. and Bard, J. B. L. (2003). The growth and morphogenesis of the early mouse mandible: a quantitative analysis. *J. Anat.* **203**, 213-222.

Rangeeth, B. N., Reddy, N. V. and Moses, J. (2011). Pierre robin sequence and the pediatric dentist. *Contemp. Clin. Dent.* **2**, 222-225.

Roberts, A., Allanson, J., Jadico, S. K., Kavamura, M. I., Noonan, J., Opitz, J. M., Young, T. and Neri, G. (2006). The cardiofaciocutaneous syndrome. *J. Med. Genet.* **43**, 833-842.

Development (2015) 142, 3734-3745 doi:10.1242/dev.125328

Shaw, P. E. and Saxton, J. (2003).Ternary complex factors: prime nuclear targets for mitogen-activated protein kinases. *Int. J. Biochem. Cell Biol.* **35**, 1210-1226.

Smyth, G. K., Michaud, J. and Scott, H. S. (2005). Use of within-array replicate spots for assessing differential expression in microarray experiments. *Bioinformatics* **21**, 2067-2075.

Song, Z., Liu, C., Iwata, J., Gu, S., Suzuki, A., Sun, C., He, W., Shu, R., Li, L., Chai, Y. et al. (2013). Mice with Tak1 deficiency in neural crest lineage exhibit cleft palate associated with abnormal tongue development. *J. Biol. Chem.* **288**, 10440-10450.

Tan, T. Y., Kilpatrick, N. and Farlie, P. G. (2013). Developmental and genetic perspectives on Pierre Robin sequence. *Am. J. Med. Genet. C Semin. Med. Genet.* **163**, 295-305.

Wilkinson, D. G. (1992). Whole mount in situ hybridization of vertebrate embryos. In *In Situ Hybridization* (ed. D. D. Wilkinson), pp. 75-83. Oxford: IRL Press.

Xu, X., Bringas, P., Soriano, P. and Chai, Y. (2005). PDGFR-α signaling is critical for tooth cusp and palate morphogenesis. *Dev. Dyn.* **232**, 75-84.

Yu, K. and Ornitz, D. M. (2011). Histomorphological study of palatal shelf elevation during murine secondary palate formation. *Dev. Dyn.* **240**, 1737-1744.

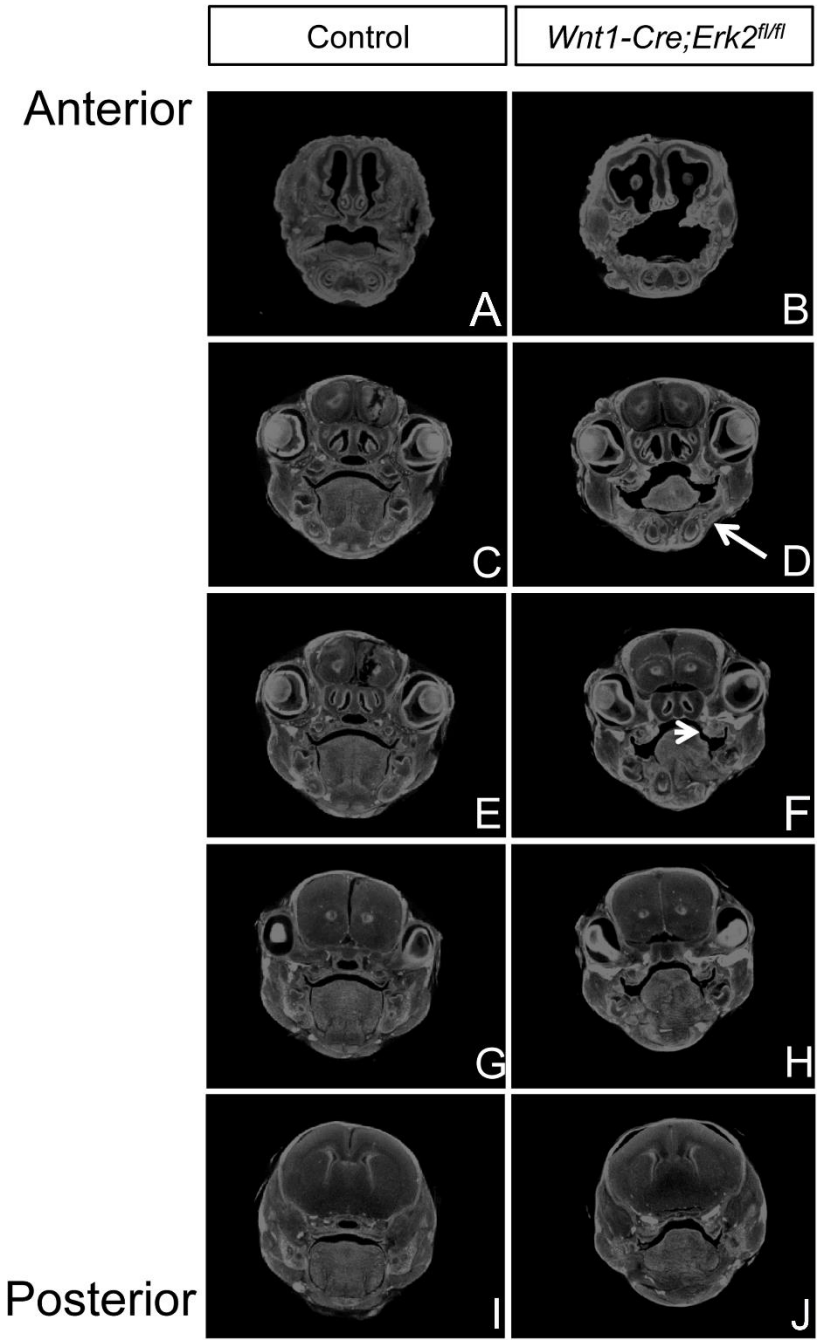

Figure S1. Palatal shelf elevation is affected along the anterior-posterior axis in *Wnt1-Cre;Erk2$^{fl/fl}$* mice. A-J. MicroCT scan sections of anterior, medial, and posterior regions of newborn control and *Wnt1-Cre;Erk2$^{fl/fl}$* mice. Arrow indicates the most affected side. Arrowheads indicate the unelevated palatal shelf.

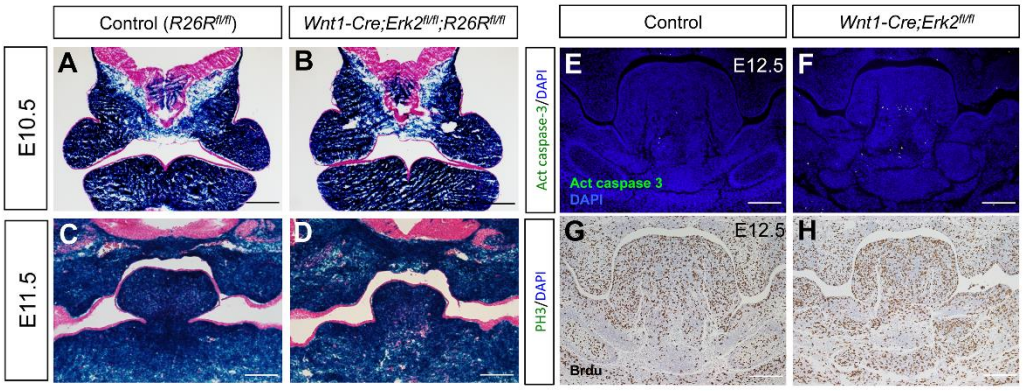

Figure S2. NCC migration, cell survival, and proliferation are unaffected in the palatal mesenchyme of *Wnt1-Cre;Erk2$^{fl/fl}$* mice. A-D. LacZ staining (blue) of coronal sections of control and *Wnt1-Cre;Erk2$^{fl/fl}$;R26R$^{fl/fl}$* embryos at E10.5 and E11.5. **E-H**. Active Caspase-3 (green) and BrdU immunostaining (brown) of E12.5 control and *Wnt1-Cre;Erk2$^{fl/fl}$* palates. Scale bars: 100 μm. n = 3 for each stage and analysis.

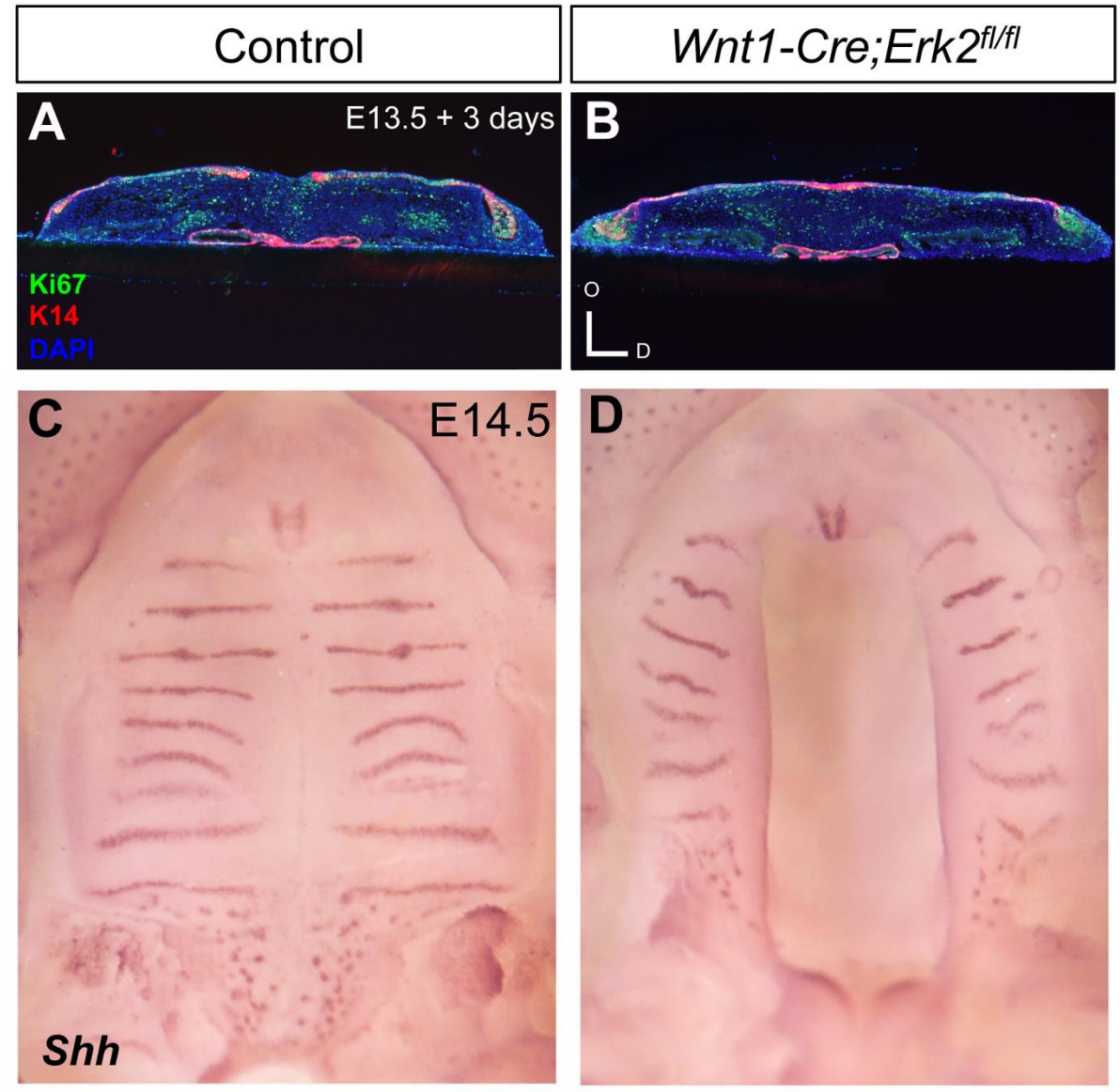

Figure S3. Midline epithelium cell fate and anterior-posterior patterning are unaffected in the palatal epithelium of *Wnt1-Cre;Erk2$^{fl/fl}$* mice. A-B. Ki67 (green) and K14 (red) double immunostaining of coronal sections of palatal explants from control and *Wnt1-Cre;Erk2$^{fl/fl}$* embryos after a 3-day incubation period. n = 4. **C-D.** *Shh in situ* hybridization in the palatal shelves of E14.5 control and *Wnt1-Cre;Erk2$^{fl/fl}$* embryos. n = 3.

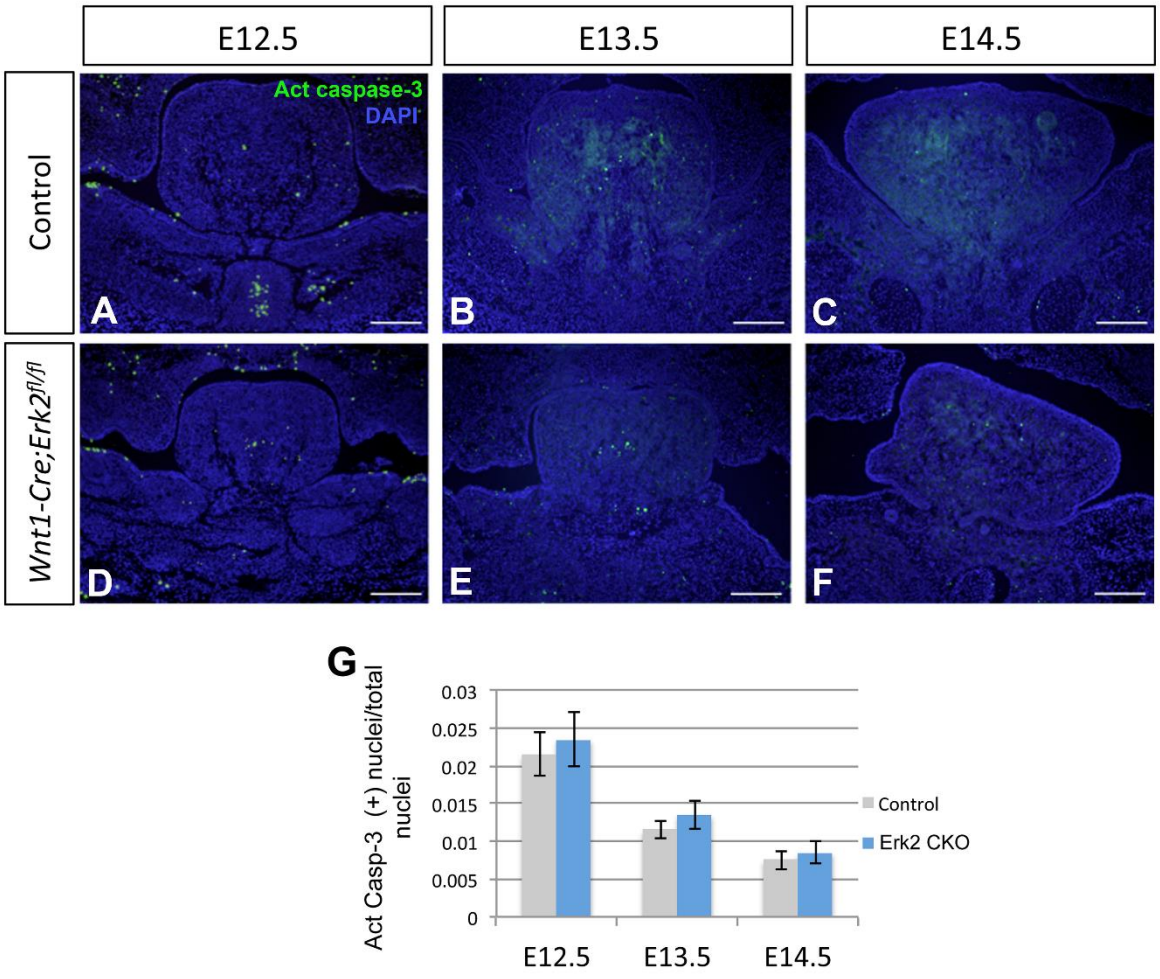

Figure S4. Apoptosis and proliferation are unaffected in the tongues of *Wnt1-Cre;Erk2$^{fl/fl}$* mice. A-F. Active Caspase-3 immunostaining (green) of coronal sections of control and *Wnt1-Cre;Erk2$^{fl/fl}$* tongues from E12.5 to E14.5. **G.** Quantification of apoptotic cells from A-F. Scale bars: 100 μm. n = 3 for each stage.

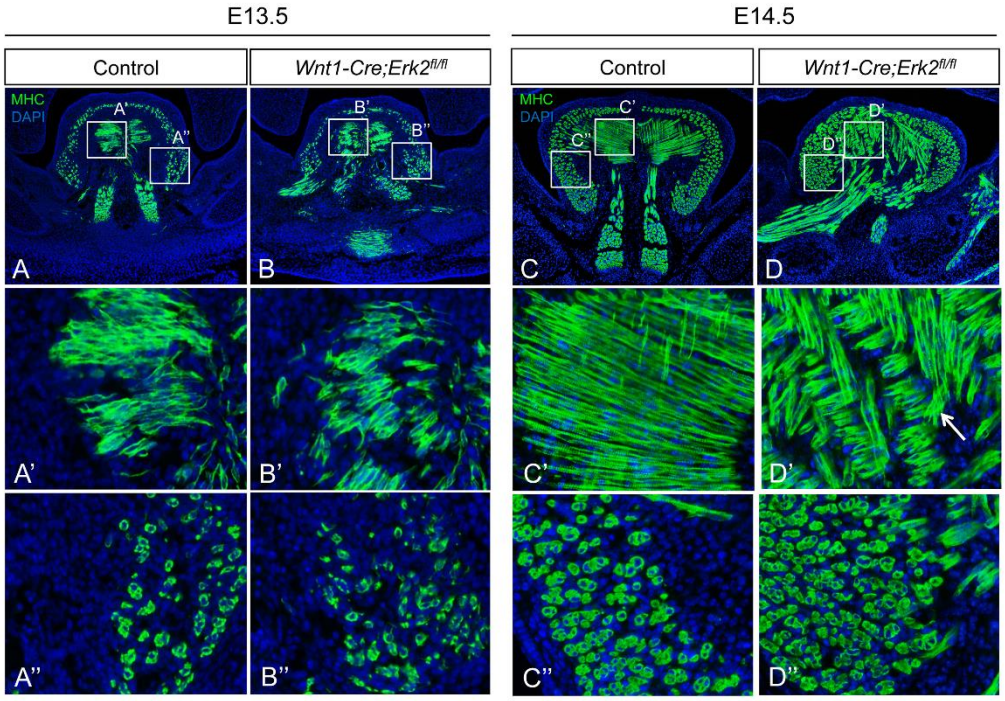

Figure S5. Differentiation is unaffected in *Wnt1-Cre;Erk2$^{fl/fl}$* tongues but muscle pattern and fiber organization are altered. A-B. MHC immunostaining (green) of coronal sections of E13.5 control and *Wnt1-Cre;Erk2$^{fl/fl}$* tongues. **C-D**. MHC immunostaining of coronal sections of E14.5 control and *Wnt1-Cre;Erk2$^{fl/fl}$* tongues. **A'-D'** and **A"-D"** are magnified images of the intrinsic muscles of the tongue at both stages. Arrow points to severe misorientation of the intrinsic muscles of the tongue.

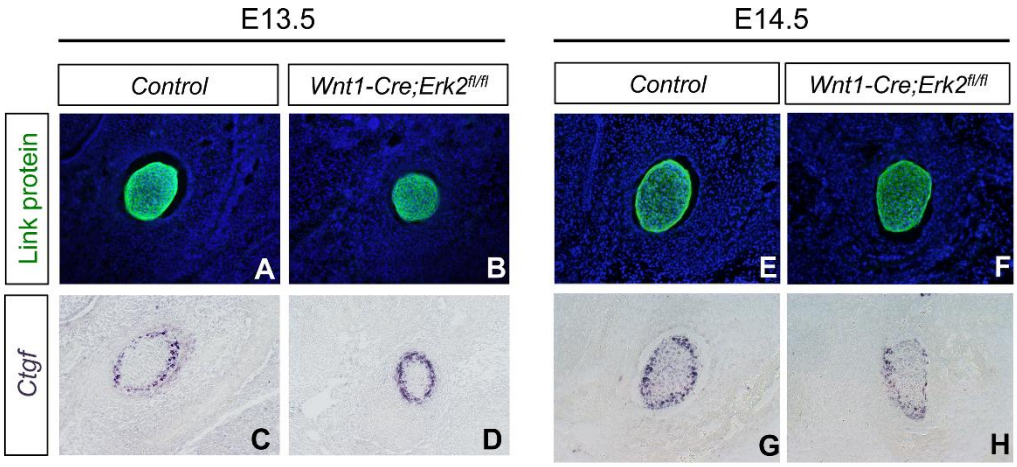

Figure S6. Chondrogenesis is unaffected in the Meckel's cartilage of *Wnt1-Cre;Erk2$^{fl/fl}$* mice. Immunostaining of Link protein (green; **A-B, E-F)** and *in situ* hybridization of *Ctgf* (**C-D**, **G-H**) in the Meckel's cartilage of E13.5 and E14.5 control and *Wnt1-Cre;Erk2$^{fl/fl}$* mice. n = 3 for each stage and analysis.

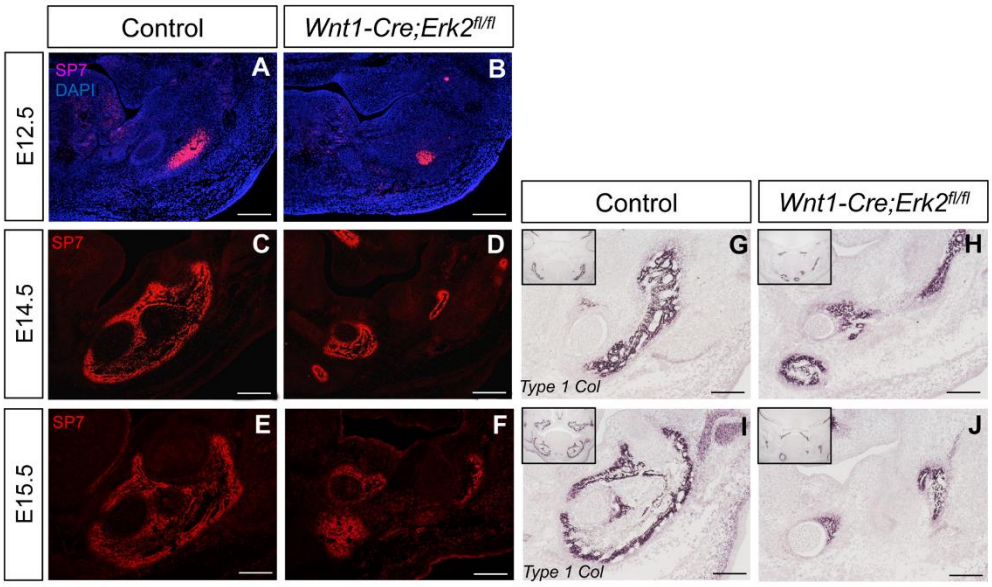

Figure S7. Population of osteogenic progenitors in *Wnt1-Cre;Erk2$^{fl/fl}$* mandibles is reduced. A-B. SP7 immunostaining (red) of mandibles in control and *Wnt1-Cre;Erk2$^{fl/fl}$* mice at E12.5. **C-F.** SP7 immunostaining (red) of mandibles in control and *Wnt1-Cre;Erk2$^{fl/fl}$* mice at E14.5 and E15.5. **G-J.** *In situ* hybridization of *Type 1 Collagen* in mandibles of control and *Wnt1-Cre;Erk2$^{fl/fl}$* mice at E14.5 and E15.5. Insets show low magnification. Scale bars: 200 μm. n = 3 for each stage and analysis.

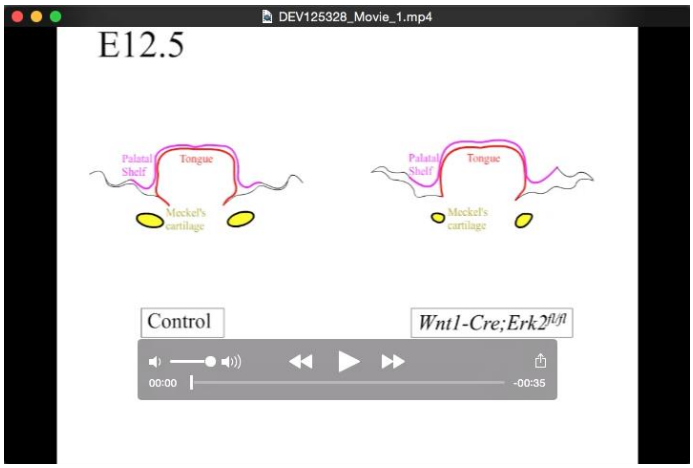

Movie 1. Comparison of control and *Wnt1-Cre;Erk2*$^{fl/fl}$ mice from E12.5 to E16.5 showing an interconnection between the palate, tongue, and mandible.

Table S1. Quantification of the mandibular phenotype in *Wnt1-Cre;Erk2*$^{fl/fl}$ mice at different stages. 72% of the cases were asymmetric. The presence, size, and continuity of the Meckel's cartilage and the osteogenic front were taken into account to determine the most affected side.

Phenotype	**E14.5**	**E15.5**	**E16.6**	**E18.5**	**P0**	**Total**
Symmetric	6	3			2	11 (27.5%)
Asymmetric (left)	7	3	2	1	3	16 (40%)
Asymmetric (right)	7	4		1	1	13 (32.5%)

Table S2. Differentially expressed transcripts in the palate of *Wnt1-Cre;Erk2*$^{fl/fl}$ mice at E13.5. Transcripts were selected by identifying those having a fold change > 1.5 and FDR < 0.05 in *Wnt1-Cre;Erk2*$^{fl/fl}$ (mutant) versus *Erk2*$^{fl/fl}$ (control) mice, as described in the Methods section. Geometric means are given for the expression values over all samples in either group.

Affymetrix ID	Gene Symbol	Mutant Geo. Mean	Wild-Type Geo. Mean	Fold Change	Adjusted *p*-value
1435239_at	Gria1	15.399	37.352	-2.426	0.005
1424609_a_at	Gm4354	114.374	253.077	-2.213	0.018
1448972_at	Gria1	20.390	45.025	-2.208	0.004
1436596_at	H2afv	53.789	112.328	-2.088	0.000
1419728_at	Cxcl5	37.211	72.088	-1.937	0.000
1428029_a_at	H2afv	1201.342	2072.950	-1.726	0.001
1440495_at	Rmst	6.998	11.450	-1.636	0.044
1429685_at	Gabrb2	26.636	43.574	-1.636	0.036
1439566_at	Gprin3	6.314	10.176	-1.612	0.044
1416298_at	Mmp9	46.968	75.632	-1.610	0.003
1436294_at	Ankrd29	17.983	28.240	-1.570	0.004
1438278_a_at	Cwc22	84.357	131.007	-1.553	0.014
1424208_at	Ptger4	67.176	103.484	-1.540	0.020
1449393_at	Sh2d1a	5.947	8.962	-1.507	0.047
1438644_x_at	Commd9	154.752	101.786	1.520	0.012
1444596_at	Pax7	12.423	8.097	1.534	0.012
1432393_a_at	Thg1l	55.881	34.495	1.620	0.029
1436279_at	Slc26a7	27.772	16.842	1.649	0.002
1419391_at	Myog	267.428	159.295	1.679	0.047
1456242_at	Gm7325	70.584	37.144	1.900	0.018
1438799_at	Dlx6os1	16.296	8.440	1.931	0.007
1450708_at	Scg2	16.200	7.235	2.239	0.009
1456498_at	Itga4	12.810	5.209	2.459	0.011

Table S3. Differentially expressed transcripts in the palate of *Wnt1-Cre;Erk2*$^{fl/fl}$ mice at E14.5. Transcripts were selected by identifying those having a fold change > 1.5 and FDR < 0.05 in *Wnt1-Cre;Erk2*$^{fl/fl}$ (mutant) versus *Erk2*$^{fl/fl}$ (control) mice, as described in the Methods section. Geometric means are given for the expression values over all samples in either group.

Affymetrix ID	Gene Symbol	Mutant Geo. Mean	Wild-Type Geo. Mean	Fold Change Mutant/WT	Adjusted *p*-value
1449880_s_at	*Bglap*	9.936	28.680	-2.887	0.027
1421979_at	*Phex*	61.451	143.278	-2.332	0.038
1436528_at	*Kazald1*	53.605	119.200	-2.224	0.035
1429379_at	*Lyve1*	22.062	46.699	-2.117	0.003
1449417_at	*Ambn*	20.122	41.673	-2.071	0.045
1436521_at	*Slc36a2*	4.074	8.128	-1.995	0.020
1434990_at	*Ppm1e*	13.965	23.799	-1.704	0.009
1453128_at	*Lyve1*	4.208	7.071	-1.680	0.004
1429029_at	*Sgms2*	14.481	24.257	-1.675	0.048
1440216_at	*Ifitm5*	303.906	498.076	-1.639	0.030
1418425_at	*Sp7*	87.579	142.708	-1.629	0.026
1440962_at	*Slc8a3*	158.301	257.463	-1.626	0.032
1443921_at	*Ranbp3l*	2.357	3.787	-1.607	0.038
1428663_at	*Sgms2*	414.976	652.834	-1.573	0.008
1419295_at	*Creb3l1*	26.854	41.519	-1.546	0.041
1429571_a_at	*Spaca1*	8.420	12.958	-1.539	0.025
1430030_at	*5330426P16Rik*	57.575	38.333	1.502	0.000
1441975_at	*Acpp*	17.176	11.358	1.512	0.014
1423935_x_at	*Krt14*	649.725	422.700	1.537	0.000
1418831_at	*Pkp3*	21.271	13.792	1.542	0.031
1418572_x_at	*Tnfrsf12a*	59.125	38.129	1.551	0.001
1422324_a_at	*Pthlh*	164.839	106.171	1.553	0.002
1435697_a_at	*Cytip*	6.179	3.977	1.554	0.041
1448612_at	*Sfn*	29.001	18.621	1.557	0.000
1424976_at	*Rhov*	17.152	10.944	1.567	0.006
1449166_at	*S100a14*	77.994	49.566	1.574	0.002
1421752_a_at	*Serpinb5*	59.531	37.777	1.576	0.006
1418449_at	*Lad1*	12.060	7.635	1.580	0.000
1457044_at	*Macc1*	44.971	28.427	1.582	0.003
1418608_at	*Calml3*	15.315	9.639	1.589	0.012
1431786_s_at	*1190003J15Rik*	18.267	11.455	1.595	0.026
1417275_at	*Mal*	47.644	29.591	1.610	0.034
1429844_at	*2310043J07Rik*	43.274	26.621	1.626	0.040
1460347_at	*Krt14*	269.001	165.345	1.627	0.000

1455893_at	*Rspo2*	42.995	26.349	1.632	0.014
1422784_at	*Krt6a*	270.447	164.546	1.644	0.001
1418350_at	*Hbegf*	21.971	13.365	1.644	0.000
1419549_at	*Arg1*	5.929	3.544	1.673	0.022
1418571_at	*Tnfrsf12a*	37.805	22.447	1.684	0.013
1454904_at	*Mtm1*	18.767	11.116	1.688	0.014
1434145_s_at	*Serhl*	21.612	12.544	1.723	0.036
1418203_at	*Pmaip1*	25.476	14.756	1.726	0.028
1417013_at	*Hspb8*	96.335	55.741	1.728	0.000
1423271_at	*Gjb2*	56.301	31.802	1.770	0.018
1422790_at	*Nppc*	5.686	3.157	1.801	0.000
1427527_a_at	*Pthlh*	32.426	17.384	1.865	0.027
1422783_a_at	*Krt6a*	43.141	22.538	1.914	0.000
1435831_at	*Upk1b*	22.911	11.647	1.967	0.003
1424890_at	*Bnc1*	28.514	13.625	2.093	0.006
1416930_at	*Ly6d*	37.975	15.326	2.478	0.000
1421551_s_at	*Ifi202b*	21.030	5.785	3.635	0.000
1457666_s_at	*Ifi202b*	57.494	11.433	5.029	0.000